Semi-Analytical Modelling of Thin-Walled Structures: Theory and Practice

2026 Edition

$$\delta\Pi = \delta U + \delta V = \{\delta c\}^T\{R\}$$
$$\delta^2\Pi = \delta(\delta U + \delta V) = 0$$

$$u(x,\theta,z,t) = u_0(x,\theta,t) + z\phi_x(x,\theta,t)$$
$$v(x,\theta,z,t) = v_0(x,\theta,t) + z\phi_\theta(x,\theta,t)$$
$$w(x,\theta,z,t) = w_0(x,\theta,t)$$
$$\phi_x = -w_{,x}$$
$$\phi_\theta = -\frac{1}{r}w_{,\theta} + \delta_1\frac{v}{r}cos\,\alpha$$

$$\delta U = \int_{\mathcal{V}} \{\delta\varepsilon\}^{\mathrm{T}}\{\sigma\}\,\mathrm{d}\mathcal{V}$$
$$\delta V = -\{\delta c\}^T\left(\{F_{ext_0}\} + \lambda\{F_{ext_\lambda}\}\right)$$

$$\{u\} \approx [g]\{c\}$$

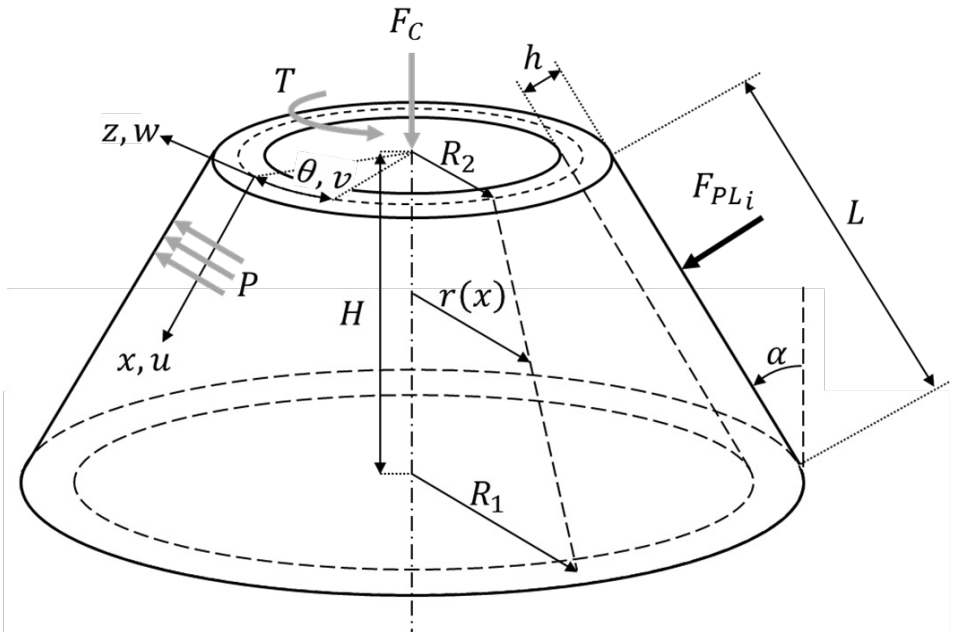

Saullo G. P. Castro

This page is intentionally left blank.

Buckling handbook

Saullo G. P. Castro

25th Mar, 2026

Keywords Buckling, Post-Buckling, Semi-Analytical, Jupyter Book, Open Science, TU Delft

This page is intentionally left blank.

Contents

Preface

This book is a successful attempt to organise all material I have concerning semi-analytical modelling, consisting of a self-contained theoretical and practical reference for young and experienced engineers and scienties. It covers topics from linear static analysis using classical formulation to deep post-buckling analysis using third-order shear deformation theory.

You will see that my focus is on displacement-based semi-analytical methods, but some special attention is given to hybrid methods approximating both the displacement and stresses, which clealry show to be advantageous for post-buckling, especially when using perturbation-based methods, such as the Koiter method.

The book is in constant development and the plan is to have one yearly official release.

Why do you call this semi-analytical instead of numerical?

In a purely numerical approach, such as finite elements (FE), smoothed particle hydrodynamics (SPH) and so forth, the domain is approximated using functions of a chosen order that have local support. For instance, a quadrilateral 4-node FE usually approximates the displacements and rotations linearly between nodes. In SPH, usually cubic- or quintic-splines are used to interpolate material-point field variables that are stored in each particle. From ththese interpolation schemes, such as FE or SPH, one can numerically solve for the displacement fields, statically or dynamically.

However, in semi-analytical methods the domain is solved with kinematic equations (strain-displacement relations) that are usually exact for a specific geometry, which is usually a plate or a shell, by means of approximation functions that pertain to the entire domain, hence having global support. This global support means that, if the systems is integrated numerically, every integration point affects all degrees-of-freedom of the corresponding domain. This is contrastingly different than FE or SPH methods, whereby an integration point only affects the corresponding local support. The ``semi-'' from ``semi-analytical'' can come from numerically integrating the domain, which is needed in non-linear analysis or on systems with arbitrarily variable stiffness or variable inertia, or it can come from the solution step, which is faster when done numerically than analytically for larger-rank systems.

Why should you learn about semi-analytical modelling?

The simplest buckling case consists of the classical solution for the deflection w of a plate with length a, width b and thickness h, under in-plane distributed loads (N_x, N_y, N_{xy}). The governing equation for this problem is given below (Kassapoglou, 2013):

$$\begin{aligned} D_{11}\frac{\partial^4 w}{\partial x^4} + 4D_{16}\frac{\partial^4 w}{\partial x^3 \partial y} \\ +2(D_{12}+2D_{66})\frac{\partial^4 w}{\partial x^2 \partial y^2} \\ +4D_{26}\frac{\partial^4 w}{\partial x \partial y^3} + D_{22}\frac{\partial^4 w}{\partial y^4} \\ = N_x\frac{\partial^2 w}{\partial x^2} + N_y\frac{\partial^2 w}{\partial y^2} + 2N_{xy}\frac{\partial^2 w}{\partial x \partial y} \end{aligned} \tag{0.1}$$

Even for this simple case, the presence of the bending-twisting coupling terms (D_{16} and D_{26}); or the laminate being not symmetric $\boldsymbol{B} \neq 0$; or boundary conditions combining, clamped, simply-supported and free edges; or if the distributed in-plane loads N_x, N_y or N_{xy} are non-constant; the buckled mode shape will skew such that the exact closed-form solutions, for instance using orthogonal Fourier series, will become intractable, requiring semi-analytical methods or finite element discretizations.

PDF and web version

The web version of the Buckling Handbook is available online at: https://saullocastro.github.io/buckling/.

The GitHub repository is available online at: https://github.com/saullocastro/buckling/.

1 Basic principles

This first chapter presents the basic principles used to produce the system of equations to be solved.

1.1 Principle of minimum potential energy

The total potential energy V can be decomposed into elastic energy U, and the work due to external forces W_{ext}:

$$V = U - W_{ext}$$

This potential becomes stationary when:

$$\delta V = \delta U - \delta W_{ext} = 0$$

1.1.1 Strain Energy

The general expression for the strain energy when $\boldsymbol{\sigma}$ increases linearly with $\boldsymbol{epsilon}$ is:

$$U = \frac{1}{2} \int_{\Omega} \boldsymbol{\sigma}^{\top} \varepsilon \, d\Omega$$

The variation of this expression, valid also for the case of $\boldsymbol{\sigma}$ being a non-linear function of ε, renders:

$$\delta U = \int_{\Omega} \boldsymbol{\sigma}^{\top} \delta\varepsilon \, d\Omega$$

To calculate the strain energy in semi-analytical formulations of plates and shells, it is convenient to represent the second-order tensors of strain and stress are represented as vectors, according to Voigt's notation (Voigt, 1910).

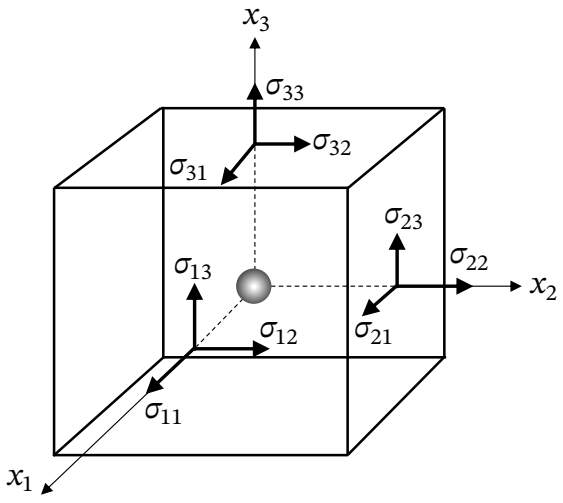

Figure 1: Complete stress state of a material point.

Given the 3D stress state of a material point illustrated in Figure 1, the components of the stress tensor σ_{ij} can be aligned in a vector as in Eq. (1.1).

$$\boldsymbol{\sigma} = \begin{Bmatrix} \sigma_{11} \\ \sigma_{22} \\ \sigma_{33} \\ \sigma_{23} \\ \sigma_{13} \\ \sigma_{12} \end{Bmatrix} \tag{1.1}$$

where:

- σ_{11} - Normal in x_1
- σ_{22} - Normal in x_2
- σ_{33} - Normal in x_3 (thickness direction)
- τ_{23} - Transverse shear 23
- τ_{13} - Transverse shear 13
- τ_{12} - In-plane shear 12

A general constitutive relation for semi-analytical models, which show stresses relate to strains, can be written based on Voigt's notation:

$$\boldsymbol{\sigma} = \boldsymbol{C}\boldsymbol{\varepsilon} \tag{1.2}$$

where $\boldsymbol{C}$ is the constitutive matrix.

Not all stress components shown in Eq. are relevant when calculating thin-walled structures. For plane stress using the Classical Laminated Plate Theory (CLPT):

$$\varepsilon_{xx}, \varepsilon_{yy}, \gamma_{xy}, \sigma_{xx}, \sigma_{yy}, \tau_{xy}$$

$$\boldsymbol{\varepsilon}^\top = \{\varepsilon_{xx} \quad \varepsilon_{yy} \quad \gamma_{xy}\} \qquad \boldsymbol{\sigma}^\top = \{\sigma_{xx} \quad \sigma_{yy} \quad \tau_{xy}\}$$

For plane stress using the First- or Third-order Shear Deformation Theory (FSDT or TSDT):

$$\varepsilon_{xx}, \varepsilon_{yy}, \gamma_{xy}, \gamma_{yz}, \gamma_{xz}$$

$$\sigma_{xx}, \sigma_{yy}, \tau_{xy}, \tau_{yz}, \tau_{xz}$$

$$\boldsymbol{\varepsilon}^\top = \{\varepsilon_{xx} \quad \varepsilon_{yy} \quad \gamma_{xy} \quad \gamma_{yz} \quad \gamma_{xz}\} \qquad \boldsymbol{\sigma}^\top = \{\sigma_{xx} \quad \sigma_{yy} \quad \tau_{xy} \quad \tau_{yz} \quad \tau_{xz}\}$$

The strains are usually expressed in terms of displacements in the so called kinematic equations, which can be generally written using Voigt's notation as:

$$\boldsymbol{\varepsilon} = \boldsymbol{B}\boldsymbol{u}$$

where $\boldsymbol{B} \equiv$ differentiation operator matrix, $\boldsymbol{u}(x, y, z) \equiv$ continuous displacement field.

Finite elements In finite elemets, interpolation functions are used to approximate the displacement field within each finite element, which can be generally written as:

$$\boldsymbol{u} = \begin{Bmatrix} u(x,y,z) \\ v(x,y,z) \\ w(x,y,z) \end{Bmatrix} = \boldsymbol{S}(x,y,z)\,\bar{\boldsymbol{u}}$$

where $\bar{\boldsymbol{u}} \equiv$ nodal displacements and $\boldsymbol{S}(x,y,z) \equiv$ interpolation (shape) functions valid only within the domain of one finite element.

Example for quadrilateral elements:

$$\boldsymbol{u} = \boldsymbol{S}_1\bar{\boldsymbol{u}}_1 + \boldsymbol{S}_2\bar{\boldsymbol{u}}_2 + \boldsymbol{S}_3\bar{\boldsymbol{u}}_3 + \boldsymbol{S}_4\bar{\boldsymbol{u}}_4$$

From the kinematic equations: $\boldsymbol{\varepsilon} = \boldsymbol{B}\boldsymbol{u}$, the differentiation operator $\boldsymbol{B}$ will contain the proper derivatives of the interpolation functions corresponding to a given finite element.

The stress strain relation $\boldsymbol{\sigma} = \boldsymbol{C}\boldsymbol{\varepsilon}$ will highly depend on each case. For trusses and beam (uniaxial stress), it can be simply $\sigma_{xx} = E\varepsilon_{xx}$, for plates this becomes more complicated, as covered later.

In finite elements, the strain energy can be thus expressed as:

$$\delta U = \int_\Omega \boldsymbol{\sigma}^\top \delta\boldsymbol{\varepsilon}\, d\Omega$$

Replacing $\boldsymbol{\sigma} = \boldsymbol{C}\boldsymbol{\varepsilon}$, for $\boldsymbol{C} = \boldsymbol{C}^\top$:

$$\delta U = \int_\Omega \boldsymbol{\varepsilon}^\top \boldsymbol{C}\,\delta\boldsymbol{\varepsilon}\, d\Omega$$

Replacing and $\boldsymbol{\varepsilon} = \boldsymbol{B}\bar{\boldsymbol{u}}$:

$$\delta U = \bar{\boldsymbol{u}}^\top \int_\Omega \boldsymbol{B}^\top \boldsymbol{C}\,\boldsymbol{B}\, d\Omega\, \delta\bar{\boldsymbol{u}}$$

$$\delta U = \bar{\boldsymbol{u}}^\top \boldsymbol{K}\,\delta\bar{\boldsymbol{u}}$$

where $\boldsymbol{K}$ is the constitutive stiffness matrix, usually referred to as simply the stiffness matrix:

$$\boldsymbol{K} = \int_\Omega \boldsymbol{B}^\top \boldsymbol{C}\,\boldsymbol{B}\, d\Omega$$

For finite elements, the rows and columns of $\boldsymbol{K}$ correspond to the degrees-of-freedom built by the assembly of all finite elements. The integration over the 3-dimensional domain Ω is performed in a piece-wise manner within the domain of each finite element Ω_e.

$$\boldsymbol{K} = \sum_{e=1}^{n_e} \boldsymbol{K}_e$$

$$\boldsymbol{K}_e = \int_{\Omega_e} \boldsymbol{B}^\top \boldsymbol{C}_e\,\boldsymbol{B}\, d\Omega_e$$

The integration of $\boldsymbol{K}_e$ can be efficiently done numerically due to the local support of the integration points (only affect the stiffness of the corresponding element).

Energy-based semi-analytical methods In energy-based methods, such as the well-known Ritz method, the shape functions are expressed in terms of continuous functions instead of nodal degrees-of-freedom:

$$\boldsymbol{u} = \begin{Bmatrix} u(x,y,z) \\ v(x,y,z) \\ w(x,y,z) \end{Bmatrix} = \boldsymbol{S}(x,y,z)\,\bar{\boldsymbol{c}}$$

where $\bar{\boldsymbol{c}} \equiv$ amplitude of each term of the shape functions, $\boldsymbol{S}(x,y,z) \equiv$ shape functions valid within the entire domain of the semi-analytical model, which can be an entire plate, an entire shell, or parts of a structure in the case of multi-domain semi-analytical models.

Example for deflection of simply supported plate $\xi = x/a$, $\eta = y/b$:

$$w(x,y) = \sum_{i=1}^{m}\sum_{j=1}^{n} c_{ij} \sin i\pi\xi \sin j\pi\eta = [\sin i\pi\xi \sin \pi\eta \quad \sin i\pi\xi \sin 2\pi\eta \quad \cdots] \begin{Bmatrix} c_{11} \\ c_{12} \\ \vdots \end{Bmatrix}$$

$$\bar{\boldsymbol{c}} = \begin{Bmatrix} c_{11} \\ c_{12} \\ \vdots \end{Bmatrix}$$

From the kinematic equations: $\varepsilon = \boldsymbol{B}\boldsymbol{u}$, the differentiation operator $\boldsymbol{B}$ will contain the proper derivatives of the shape functions.

The strain energy for the Ritz method can thus be expressed as:

$$\delta U = \int_{\Omega} \boldsymbol{\sigma}^{\top}\, \delta\varepsilon \, d\Omega$$

Replacing $\boldsymbol{\sigma} = \boldsymbol{C}\varepsilon$, for $\boldsymbol{C} = \boldsymbol{C}^{\top}$:

$$\delta U = \int_{\Omega} \varepsilon^{\top} \boldsymbol{C}\, \delta\varepsilon \, d\Omega$$

Replacing and $\varepsilon = \boldsymbol{B}\boldsymbol{c}$:

$$\delta U = \boldsymbol{c}^{\top} \int_{\Omega} \boldsymbol{B}^{\top} \boldsymbol{C}\, \boldsymbol{B}\, d\Omega\, \delta\boldsymbol{c}$$

$$\delta U = \boldsymbol{c}^{\top} \boldsymbol{K}\, \delta\boldsymbol{c}$$

with the constitutive stiffness matrix defined as:

$$\boldsymbol{K} = \int_{\Omega} \boldsymbol{B}^{\top} \boldsymbol{C}\, \boldsymbol{B}\, d\Omega$$

In the Ritz Method, the rows and columns of $\boldsymbol{K}$ correspond to the degrees-of-freedom that depend on the number of function terms used in the displacement approximation. In single-domain semi-analytical models, there is only one integration domain Ω, and the integration is usually performed analytically leading to very efficient methods that can analytically calculate the stiffness matrix, even for complex problems such as described by Castro et al. addressing the buckling of conical shells under combined load cases (Castro et al., 2014). However, when numerical integration is needed, for instance due to variable stiffness or in non-linear analyses (Castro et al., 2015b), the non-local support of the integration can create a large disadvantage of the Ritz method when compared to the finite element. The non-local support comes from the fact that the approximation functions represent the whole domain, and each integration point requires the evaluation of the

entire stiffness matrix because all degress-of-freedom are components of continuous functions that affect that integration point.

Therefore, one must be careful while implementing semi-analytical methods for cases of variable stiffness or non-linear analyses. The use of hierarchical polynomials as approximation functions enable such efficient implementations, because they allow the use of Gauss quadrature rules to efficiently perform the numerical integration. When trigonometric approximation functions are used the stiffness matrix can be integrated using the trapezoidal (piece-wise linear) or Simpson's rule (piece-wise quadratic) (Castro et al., 2015a)

1.1.2 Work due to external forces

When considering tranction stresses $\bar{\boldsymbol{\sigma}}$ acting on the boundaries of the domain $\delta\Omega$, and body forces $\boldsymbol{b}$ acting on the entire volume of the domain Ω, the following general expression for the work of external forces can be used:

$$W_{ext} = \int_{\Omega} \boldsymbol{b}^{\top} \boldsymbol{u} \, d\Omega + \int_{\delta\Omega} (\bar{\boldsymbol{\sigma}}^{\top} \boldsymbol{u}) d(\delta\Omega)$$

The first variation of work due to external forces becomes:

$$\delta W_{ext} = \int_{\Omega} \boldsymbol{b}^{\top} \delta\boldsymbol{u} \, d\Omega + \int_{\delta\Omega} (\bar{\boldsymbol{\sigma}}^{\top} \delta\boldsymbol{u}) d(\delta\Omega) = \boldsymbol{F}^{\top} \delta\boldsymbol{u}$$

where $\boldsymbol{F} \equiv$ external force vector, including body ($\boldsymbol{b}$) and boundary forces ($\bar{\boldsymbol{\sigma}}$).

1.1.3 Semi-analytical static solution

Back to the stationary total potential energy functional:

$$\delta V = \delta U - \delta W_{ext} = 0$$

The state of V depends on a nodal displacement vector $\bar{\boldsymbol{u}}$ in the case of displacement-based finite elements. In the Ritz method, we can make $\bar{\boldsymbol{c}} = \bar{\boldsymbol{u}}$ such that $\bar{\boldsymbol{u}}$ represents the Ritz coefficients $\bar{\boldsymbol{c}}$ that contain the amplitude of each term of the shape functions.

We can represent δV using Fréchet's derivatives. In the case of linear analyses:

$$\delta V = {V'}^{\top} \delta\bar{\boldsymbol{u}} = 0$$

Thus, $V' = \boldsymbol{R}$, or a residual force vector, with V' being the first Fréchet's derivative of V. Using the definition for the total potential energy, the first variation becomes:

$${V'}^{\top} \delta\bar{\boldsymbol{u}} = \int_{\Omega} \boldsymbol{\sigma}^{\top} \delta\boldsymbol{\varepsilon} \, d\Omega - \int_{\Omega} (\boldsymbol{b}^{\top} \delta\boldsymbol{u}) d\Omega - \int_{\delta\Omega} (\bar{\boldsymbol{\sigma}}^{\top} \delta\boldsymbol{u}) d(\delta\Omega) = 0$$

1.2 Approximation functions

The orthogonal trigonometric series is the simplest solution for Eq. (0.1).

$$w = \sum_{m=1}^{\infty} \sum_{n=1}^{\infty} A_{mn} \sin\left(\frac{m\pi x}{a}\right) \sin\left(\frac{n\pi y}{b}\right)$$

However, when a general set of boundary conditions is needed, or whenever a skewed buckling mode is possible, a more robust approximation for the displacement field is required. Castro and

Donadon (Castro and Donadon, 2017) present Rodrigues' form of Legendre hierarchic orthogonal polynomials (Peano, 1976; De-Chao, 1986), largely applied by Bardell et al. on the vibration problems (Bardell, 1991; Bardell et al., 1997b,a). In this form the first four terms $i = 1, 2, 3, 4$ consist of Hermite cubic polynomials:

$$P_1(\chi) = \left(\frac{1}{2} - \frac{3}{4}\chi + \frac{1}{4}\chi^3\right)\delta_{t1}$$
$$P_2(\chi) = \left(\frac{1}{8} - \frac{1}{8}\chi - \frac{1}{8}\chi^2 + \frac{1}{8}\chi^3\right)\delta_{r1}$$
$$P_3(\chi) = \left(\frac{1}{2} + \frac{3}{4}\chi - \frac{1}{4}\chi^3\right)\delta_{t2}$$
$$P_4(\chi) = \left(-\frac{1}{8} - \frac{1}{8}\chi + \frac{1}{8}\chi^2 + \frac{1}{8}\chi^3\right)\delta_{r2}$$

with $\chi \in \{\xi, \eta, \zeta\}$, and for any $i > 4$:

$$P_i(\chi) = \sum_{p=0}^{i/2} \frac{(-1)^p (2i - 2p - 7)!!}{2^p p!(i - 2p - 1)!} \chi^{i-2p-1}$$

where $q!! = q(q-2)\ldots(2 \text{ or } 1)$ such that $0!! = 1$, and $(i/2)$ in the summation is an integer division. The binary flags δ_{t1}, δ_{r1}, δ_{t2} and δ_{r2} are equal to 0 or 1, and used in the first four terms of Rodrigues polynomials to enable or disable the translation and rotation of each domain boundary, as illustrated in Figure 2. From the fifth term onwards, the translation and rotation at the boundaries are always zero, such that they are use to increase the interpolation order in the inner part of the domain, as illustrated in Figure 3. Flag δ_{t1} is used to control the translation at boundary ($\chi = -1$), which is possible because using Rodrigues polynomials this is the only term among all terms in the approximation function that produces $P_i(\chi = -1) = 1$. Similarly, δ_{t2} is used to control the translation at boundary 2 ($\chi = +1$). The rotation at $\chi = -1$ and $\chi = +1$ is respectively controlled using δ_{r1} and δ_{r2}, since they are the only terms that produce a non-null rotation $\partial P/\partial\chi$ at each respective domain boundary. The use of rotation is specially important in FSDT or TSDT formulations. Vescovini et al. (Vescovini et al., 2018) investigated the sparsity of the systems produced by different shape functions, positively supporting the use of these Legendre hierarchical polynomials.

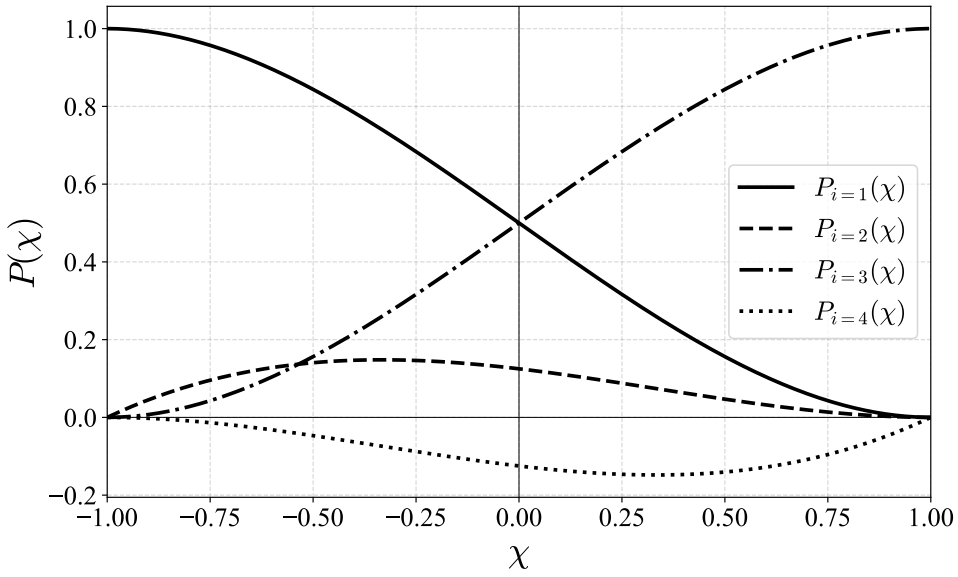

Figure 2: Legendre polynomial boundary functions.

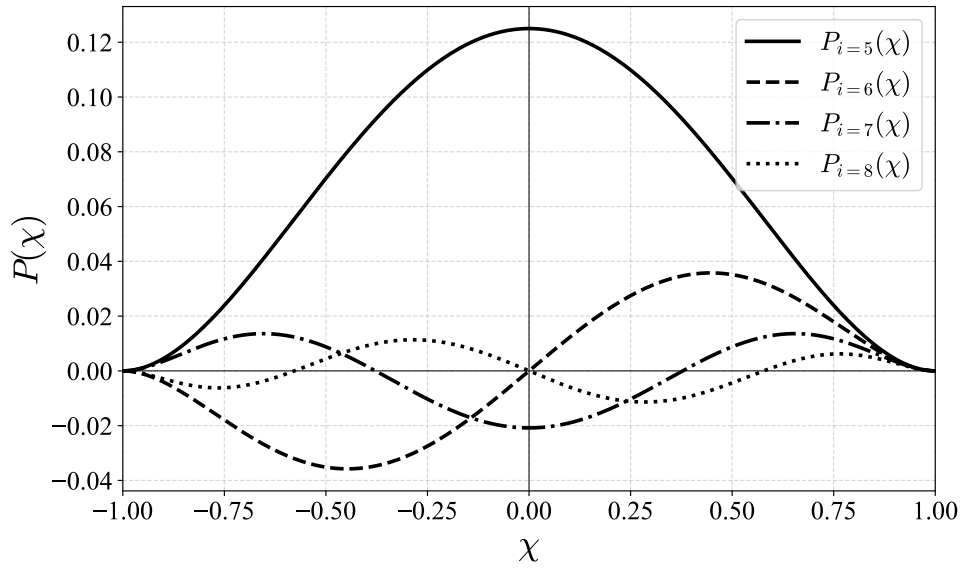

Figure 3: Legendre polynomial inner functions.

Take the plate-like domain shown in Figure 4. A general expression for the 3D displacement field is:

$$\boldsymbol{u} = \begin{Bmatrix} u(x,y,z) \\ v(x,y,z) \\ w(x,y,z) \end{Bmatrix} = \boldsymbol{S}(x,y,z)\bar{\boldsymbol{c}} = \begin{Bmatrix} \boldsymbol{S}^u(x,y,z) \\ \boldsymbol{S}^v(x,y,z) \\ \boldsymbol{S}^w(x,y,z) \end{Bmatrix} \bar{\boldsymbol{c}}$$

using Legendre polynomials and a summation convention for repeated indices:

$$u(x,y,z) = c^u_{ijk} P_i(\xi) P_j(\eta) P_k(\zeta)$$

$$v(x,y,z) = c^v_{ijk} P_i(\xi) P_j(\eta) P_k(\zeta)$$

$$w(x,y,z) = c^w_{ijk} P_i(\xi) P_j(\eta) P_k(\zeta)$$

with $1 \leq [i,j,k] \leq n_{[x,y,z]}$ where $n_[x,y,z]$ represents the number of terms in each global coordinate direction. The natural coordinates ξ, η and ζ are defined as follows for a plate:

$$\xi = \frac{2x}{a} - 1$$

$$\eta = \frac{2y}{b} - 1$$

$$\zeta = \frac{2z}{h} - 1$$

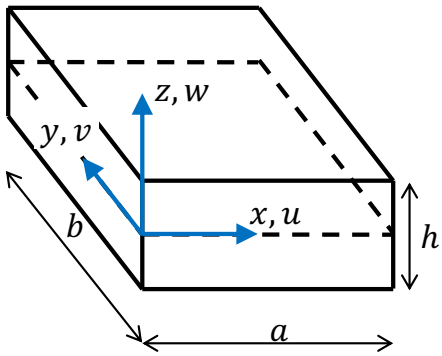

Figure 4: Three-dimensional plate domain.

For the sake of completeness, let's also write the expressions for the displacement field using explicit summation:

$$u(x,y,z) = \sum_{i=1}^{n_x} \sum_{ij=1}^{n_y} \sum_{k=1}^{n_z} c_{ijk}^{u} P_i(\xi) P_j(\eta) P_k(\zeta)$$

$$v(x,y,z) = \sum_{i=1}^{n_x} \sum_{ij=1}^{n_y} \sum_{k=1}^{n_z} c_{ijk}^{v} P_i(\xi) P_j(\eta) P_k(\zeta)$$

$$w(x,y,z) = \sum_{i=1}^{n_x} \sum_{ij=1}^{n_y} \sum_{k=1}^{n_z} c_{ijk}^{w} P_i(\xi) P_j(\eta) P_k(\zeta)$$

and using vector notation:

$$u(x,y,z) = \boldsymbol{S}^{u}\boldsymbol{c}$$

$$v(x,y,z) = \boldsymbol{S}^{u}\boldsymbol{c}$$

$$w(x,y,z) = \boldsymbol{S}^{u}\boldsymbol{c}$$

where $\boldsymbol{c}$ contains all coefficients c_{ijk} for $1 \leq [i,j,k] \leq n_{[x,y,z]}$. The sequence in which the coefficients are placed is arbitrary and does not affect the level of sparsity of the stiffness matrix or other structural matrices, but it does affect the bandwidth of these matrices, which significantly affects the overall efficiency and numerically stability of the implementation. To illustrate the differences in defree-of-freedom (DOF) ordering, a practical example of the buckling of a plate using 3D elasticity is investigated in depth in this notebook. There, the DOF are stored in a block- and alternated-based approach. The results are compared in detail, and the sparsity of the stiffness matrix $\boldsymbol{K}$ is illustrated in Figure 5. A detailed formulation of this problem is provided in details in Section 4.2.

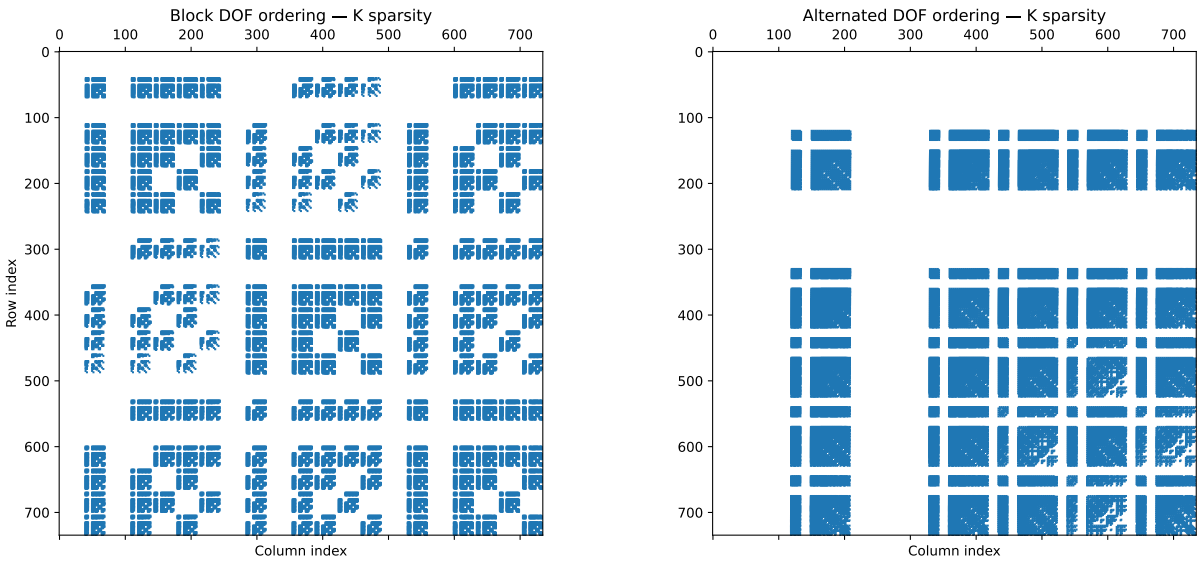

Figure 5: Degrees-of-freedom of the stiffness matrix for block and alternated approaches.

1.3 Neutral Equilibrium Criterion

The neutral equilibrium of a vertical slender beam is illustrated in Figure 6

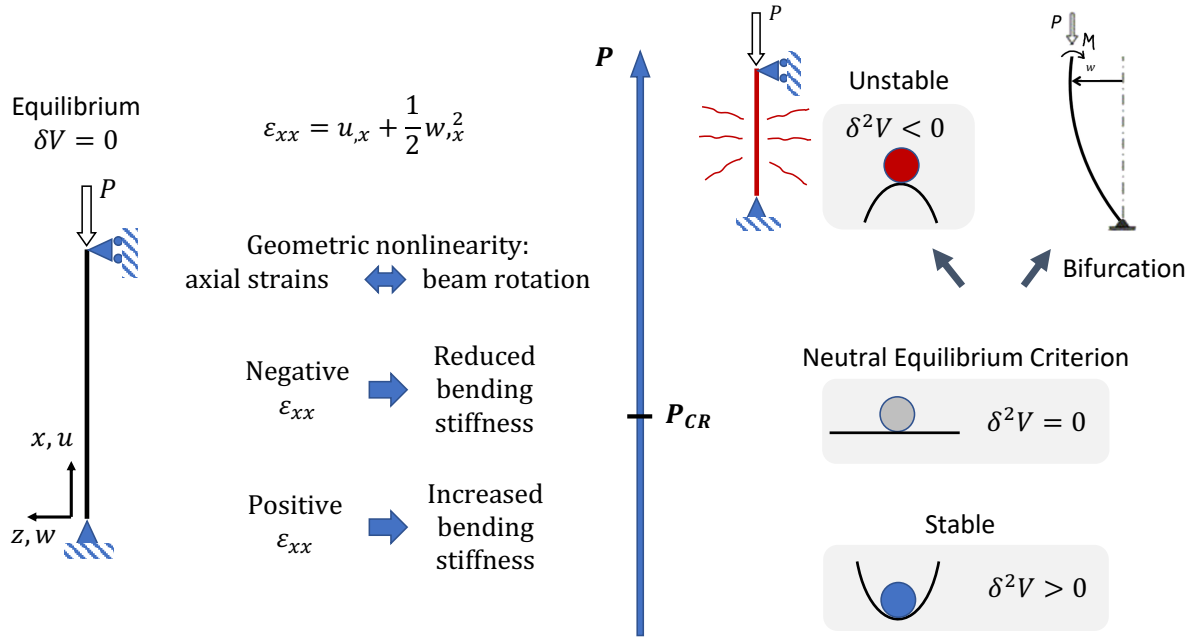

Figure 6: Neutral Equilibrium of a vertical slender beam.

Given the expression for V':

$$V'^{\top} \delta \bar{\boldsymbol{u}} = \int_{\Omega} \boldsymbol{\sigma}^{\top} \delta \varepsilon \, d\Omega - \int_{\Omega} (\hat{\boldsymbol{b}}^{\top} \delta \boldsymbol{u}) d\Omega - \int_{\delta\Omega} (\hat{\boldsymbol{\sigma}}^{\top} \delta \boldsymbol{u}) d(\delta\Omega)$$

The second variation of V becomes:

$$\delta^2 V = V''\delta\bar{\boldsymbol{u}}\delta\bar{\boldsymbol{u}} =$$

$$= \int_\Omega \delta\boldsymbol{\sigma}^\top \delta\boldsymbol{\varepsilon}\, d\Omega + \int_\Omega \boldsymbol{\sigma}^\top \delta^2\boldsymbol{\varepsilon}\, d\Omega - \int_\Omega (\delta\hat{\boldsymbol{b}}^\top \delta\boldsymbol{u}) d\Omega - \int_\Omega (\hat{\boldsymbol{b}}^\top \delta^2\boldsymbol{u}) d\Omega - \int_{\delta\Omega} (\delta\hat{\boldsymbol{\sigma}}^\top \delta\boldsymbol{u}) d(\delta\Omega) - \int_{\delta\Omega} (\hat{\boldsymbol{\sigma}}^\top \delta^2\boldsymbol{u}) d(\delta\Omega)$$

In a system without follower forces $\delta\hat{\boldsymbol{\sigma}} = \delta\hat{\boldsymbol{b}} = \boldsymbol{0}$, and we can consider $\delta^2\boldsymbol{u} \ll \delta\boldsymbol{u}$:

$$V''\delta\bar{\boldsymbol{u}}\delta\bar{\boldsymbol{u}} = \int_\Omega \delta\boldsymbol{\sigma}^\top \delta\boldsymbol{\varepsilon}\, d\Omega + \int_\Omega \boldsymbol{\sigma}^\top \delta^2\boldsymbol{\varepsilon}\, d\Omega$$

The first integral represents the nonlinear constitutive stiffness, whereas the second integral represents the geometric stiffness matrix. If the strains can be represented as:

$$\boldsymbol{\varepsilon} = \left(\boldsymbol{B}_L + \frac{1}{2}\boldsymbol{B}_{NL}\right)\bar{\boldsymbol{u}} \qquad \text{and} \qquad \delta\boldsymbol{\varepsilon} = (\boldsymbol{B}_L + \boldsymbol{B}_{NL})\delta\bar{\boldsymbol{u}}$$

And the stresses as:

$$\boldsymbol{\sigma} = \boldsymbol{C}\boldsymbol{\varepsilon}$$

Then:

$$V''\delta\bar{\boldsymbol{u}}\delta\bar{\boldsymbol{u}} = \delta\bar{\boldsymbol{u}}^\top \int_\Omega (\boldsymbol{B}_L + \boldsymbol{B}_{NL})^\top \boldsymbol{C}(\boldsymbol{B}_L + \boldsymbol{B}_{NL}) d\Omega\, \delta\bar{\boldsymbol{u}} + \int_\Omega \boldsymbol{\sigma}^\top \delta^2\boldsymbol{\varepsilon}\, d\Omega$$

The neutral equilibrium criterion states that:

$$\delta^2 V = 0$$

$$\delta^2 V = V''\delta\bar{\boldsymbol{u}}\delta\bar{\boldsymbol{u}} = \delta\bar{\boldsymbol{u}}^\top \int_\Omega (\boldsymbol{B}_L + \boldsymbol{B}_{NL})^\top \boldsymbol{C}(\boldsymbol{B}_L + \boldsymbol{B}_{NL}) d\Omega\, \delta\bar{\boldsymbol{u}} + \delta\bar{\boldsymbol{u}}^\top \boldsymbol{K}_G \delta\bar{\boldsymbol{u}} = 0$$

This term represents the constitutive stiffness matrix:

$$\boldsymbol{K}_C = \int_\Omega (\boldsymbol{B}_L + \boldsymbol{B}_{NL})^\top \boldsymbol{C}(\boldsymbol{B}_L + \boldsymbol{B}_{NL}) d\Omega$$

From a linear fundamental (pre-buckling) state we have that $\boldsymbol{B}_{NL} = \boldsymbol{0}$:

$$\boldsymbol{K}_C = \boldsymbol{K}_0 = \int_\Omega \boldsymbol{B}_L^\top \boldsymbol{C}\boldsymbol{B}_L d\Omega$$

such that:

$$\delta^2 V = \delta\bar{\boldsymbol{u}}^\top \boldsymbol{K}_0 \delta\bar{\boldsymbol{u}} + \delta\bar{\boldsymbol{u}}^\top \boldsymbol{K}_G \delta\bar{\boldsymbol{u}} = 0$$

where $\boldsymbol{K}_G$ represents the geometric stiffness matrix. Note that this expression must be true for any variation $\delta\bar{\boldsymbol{u}}$, such that $\boldsymbol{K}_0 + \lambda\boldsymbol{K}_G$ must be singular for the expression to be generaly true, hence:

$$\det(\boldsymbol{K}_0 + \lambda\boldsymbol{K}_G) = 0$$

where λ is a load multiplier applied to the initial stress state defining $\boldsymbol{K}_G$. This is the well-known eigenvalue problem for buckling, also referred to as linear buckling equation.

2 Strain-displacement (kinematic) equations for plates, cylindrical and spherical shells

The discussion presented by Castro (Castro, 2015, 2025) is herein expanded and detailed. A general overview from the full elasticity theory to the main equivalent single-layer (ESL) theories is given, for plates and shells, including cylindrical, conical and spherical. The ESL theories discussed are Classical Laminated Plate Theory (CLPT), First- and Third-order Shear Deformation Theories (FSDT and TSDT). Engineering shear strains are used throughout the discussion ($\gamma_{ij} = 2\varepsilon_{ij}$).

2.1 General strain-displacement relations

According to the three-dimensional (3D) elasticity theory, the strain components referred to an arbitrary orthogonal coordinate system x_1,x_2, x_3, illustrated in Figure 7

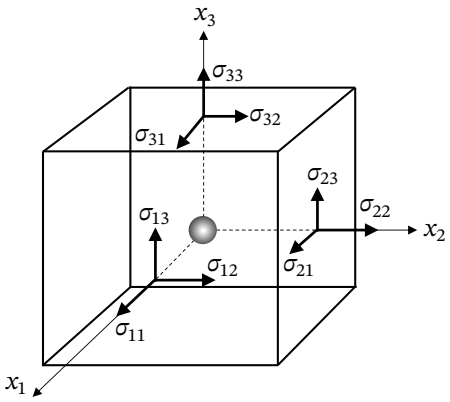

Figure 7: Complete stress state of a material point.

can be written as (Castro, 2015):

$$
\begin{aligned}
\epsilon_{11} &= \frac{1}{2}\left(\left(\frac{e_{13}}{2}-\omega_2\right)^2+\left(\frac{e_{12}}{2}+\omega_3\right)^2+e_{11}^2\right)+e_{11}\\
\epsilon_{22} &= \frac{1}{2}\left(\left(\frac{e_{23}}{2}+\omega_1\right)^2+\left(\frac{e_{12}}{2}-\omega_3\right)^2+e_{22}^2\right)+e_{22}\\
\epsilon_{33} &= \frac{1}{2}\left(\left(\frac{e_{23}}{2}-\omega_1\right)^2+\left(\frac{e_{13}}{2}+\omega_2\right)^2+e_{33}^2\right)+e_{33}\\
\epsilon_{12} &= \left(\frac{e_{23}}{2}+\omega_1\right)\left(\frac{e_{13}}{2}-\omega_2\right)+e_{11}\left(\frac{e_{12}}{2}-\omega_3\right)+e_{22}\left(\frac{e_{12}}{2}+\omega_3\right)+e_{12}\\
\epsilon_{13} &= e_{33}\left(\frac{e_{13}}{2}-\omega_2\right)+e_{11}\left(\frac{e_{13}}{2}+\omega_2\right)+\left(\frac{e_{23}}{2}-\omega_1\right)\left(\frac{e_{12}}{2}+\omega_3\right)+e_{13}\\
\epsilon_{23} &= e_{22}\left(\frac{e_{23}}{2}-\omega_1\right)+e_{33}\left(\frac{e_{23}}{2}+\omega_1\right)+\left(\frac{e_{13}}{2}+\omega_2\right)\left(\frac{e_{12}}{2}-\omega_3\right)+e_{23}
\end{aligned}
$$

where the parameters $\epsilon_i j$ and ω_i are (the conventional notation for partial derivatives $\partial/\partial x$ is used here for the sake of clarity) the following (Castro (2015)), with u, v, w being the displacements along directions x_1, x_2, x_3, respectively:

$$
\begin{aligned}
e_{11} &= \frac{1}{H_1}\frac{\partial u}{\partial x_1} + \frac{v}{H_1 H_2}\frac{\partial H_1}{\partial x_2} + \frac{w}{H_1 H_3}\frac{\partial H_1}{\partial x_3} \\
e_{22} &= \frac{u}{H_1 H_2}\frac{\partial H_2}{\partial x_1} + \frac{1}{H_2}\frac{\partial v}{\partial x_2} + \frac{w}{H_2 H_3}\frac{\partial H_2}{\partial x_3} \\
e_{33} &= \frac{u}{H_1 H_3}\frac{\partial H_3}{\partial x_1} + \frac{v}{H_2 H_3}\frac{\partial H_3}{\partial x_2} + \frac{1}{H_3}\frac{\partial w}{\partial x_3} \\
e_{12} &= \frac{H_1}{H_2}\frac{\partial}{\partial x_2}\left(\frac{u}{H_1}\right) + \frac{H_2}{H_1}\frac{\partial}{\partial x_1}\left(\frac{v}{H_2}\right) \\
e_{13} &= \frac{H_1}{H_3}\frac{\partial}{\partial x_3}\left(\frac{u}{H_1}\right) + \frac{H_3}{H_1}\frac{\partial}{\partial x_1}\left(\frac{w}{H_3}\right) \\
e_{23} &= \frac{H_2}{H_3}\frac{\partial}{\partial x_3}\left(\frac{v}{H_2}\right) + \frac{H_3}{H_2}\frac{\partial}{\partial x_2}\left(\frac{w}{H_3}\right) \\
\omega_1 &= \frac{\frac{\partial (H_3 w)}{\partial x_2} - \frac{\partial (H_2 v)}{\partial x_3}}{2(H_2 H_3)} \\
\omega_2 &= \frac{\frac{\partial (H_1 u)}{\partial x_3} - \frac{\partial (H_3 w)}{\partial x_1}}{2(H_1 H_3)} \\
\omega_3 &= \frac{\frac{\partial (H_2 v)}{\partial x_1} - \frac{\partial (H_1 u)}{\partial x_2}}{2(H_1 H_2)} \\
H_1 &= \sqrt{(X_{1,x_1})^2 + (X_{2,x_1})^2 + (X_{3,x_1})^2} \\
H_2 &= \sqrt{(X_{1,x_2})^2 + (X_{2,x_2})^2 + (X_{3,x_2})^2} \\
H_3 &= \sqrt{(X_{1,x_3})^2 + (X_{2,x_3})^2 + (X_{3,x_3})^2}
\end{aligned}
$$

2.2 3D kinematic equations for plates

Figure 8 shows the local and global coordinates of a plate.

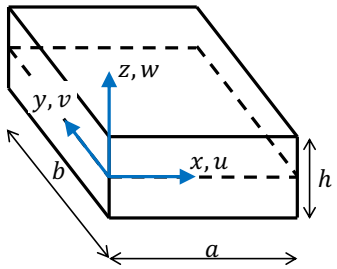

Figure 8: Plate domain.

from where the following coordinate relations can be obtained:

$$
\begin{aligned}
x_1 &= x \quad X_1 = x \\
x_2 &= y \quad X_2 = y \\
x_3 &= z \quad X_3 = z
\end{aligned}
$$

Defining:

$$\begin{aligned} \varepsilon_{xx} &= \epsilon_{11} \quad \gamma_{xy} = 2\varepsilon_{xy} = \epsilon_{12} \\ \varepsilon_{yy} &= \epsilon_{22} \quad \gamma_{xz} = 2\varepsilon_{xz} = \epsilon_{13} \\ \varepsilon_{zz} &= \epsilon_{33} \quad \gamma_{yz} = 2\varepsilon_{yz} = \epsilon_{23} \end{aligned}$$

We have that:

$$\begin{aligned} \varepsilon_{xx} &= u_{,x} + \frac{1}{2}(u_{,x}^2 + v_{,x}^2 + w_{,x}^2) \\ \varepsilon_{yy} &= v_{,y} + \frac{1}{2}(u_{,y}^2 + v_{,y}^2 + w_{,y}^2) \\ \varepsilon_{zz} &= w_{,z} + \frac{1}{2}(u_{,z}^2 + v_{,z}^2 + w_{,z}^2) \\ \gamma_{xy} &= u_{,y} + v_{,x} + (u_{,x}u_{,y} + v_{,x}v_{,y} + w_{,x}w_{,y}) \\ \gamma_{xz} &= u_{,z} + w_{,x} + (u_{,x}u_{,z} + v_{,x}v_{,z} + w_{,x}w_{,z}) \\ \gamma_{yz} &= v_{,z} + w_{,y} + (u_{,y}u_{,z} + v_{,y}v_{,z} + w_{,y}w_{,z}) \end{aligned} \tag{2.1}$$

2.3 3D kinematic equations for cylindrical shells

Figure 9 shows the local and global coordinates of a cylindrical shell.

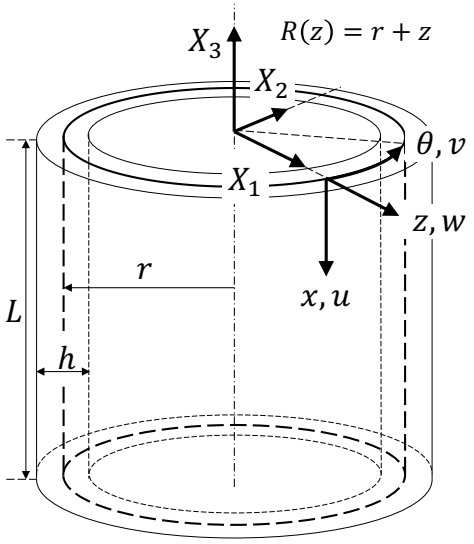

Figure 9: Cylindrical shell domain.

from where the following geometric relations can be derived (Castro, 2015):

$$\begin{aligned} x_1 &= x \quad X_1 = R(z)\cos(\theta) \\ x_2 &= \theta \quad X_2 = R(z)\sin(\theta) \\ x_3 &= z \quad X_3 = -x \end{aligned}$$

Defining:

$$\begin{aligned} \varepsilon_{xx} &= \epsilon_{11} \quad \gamma_{x\theta} = 2\varepsilon_{x\theta} = \epsilon_{12} \\ \varepsilon_{\theta\theta} &= \epsilon_{22} \quad \gamma_{xz} = 2\varepsilon_{xz} = \epsilon_{13} \\ \varepsilon_{zz} &= \epsilon_{33} \quad \gamma_{\theta z} = 2\varepsilon_{\theta z} = \epsilon_{23} \end{aligned}$$

we have that, **considering only the linear terms**:

$$\begin{aligned} \varepsilon_{xx} &= u_{,x} \\ \varepsilon_{\theta\theta} &= \frac{v_{,\theta}}{R(z)} + \frac{w}{R(z)} \\ \varepsilon_{zz} &= w_{,z} \\ \gamma_{x\theta} &= \frac{u_{,\theta}}{R(z)} + v_{,x} \\ \gamma_{xz} &= u_{,z} + w_{,x} \\ \gamma_{\theta z} &= v_{,z} + \frac{w_{,\theta}}{R(z)} - \frac{v}{R(z)} \end{aligned} \tag{2.2}$$

These equations represent the linear part of the strain-displacement relations (small strain/small displacement). The terms containing $R(z)$ in the denominators account for the curvature of the coordinate system. Specifically, the $\frac{w}{R(z)}$ term in $\varepsilon_{\theta\theta}$ represents the ``hoop strain'' contribution from radial displacement.

2.4 3D kinematic equations for conical shells

Figure 10 shows the local and global coordinates of a conical shell, adapted from Castro et al. (Castro et al., 2014, 2015a,b; Castro, 2015).

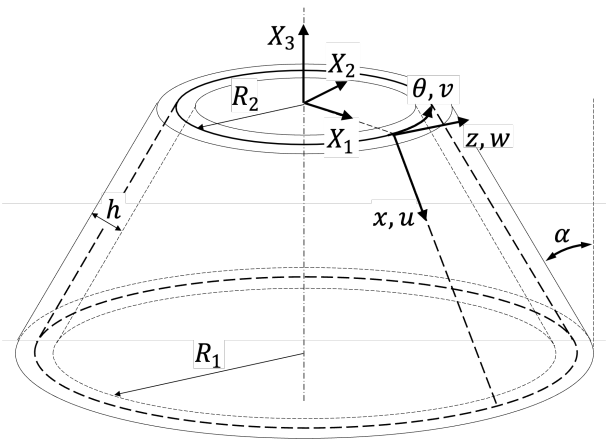

Figure 10: Conical shell domain.

from where the following geometric relations can be derived (Castro, 2015):

$$\begin{aligned} x_1 &= x \quad X_1 = R(x,z)\cos\theta \\ x_2 &= \theta \quad X_2 = R(x,z)\sin\theta \\ x_3 &= z \quad X_3 = z\sin\alpha - x\cos\alpha \\ R(x,z) &= R_2 + x\sin\alpha + z\cos\alpha \end{aligned}$$

Defining:

$$\begin{aligned} \varepsilon_{xx} &= \epsilon_{11} \quad \gamma_{x\theta} = 2\varepsilon_{x\theta} = \epsilon_{12} \\ \varepsilon_{\theta\theta} &= \epsilon_{22} \quad \gamma_{xz} = 2\varepsilon_{xz} = \epsilon_{13} \\ \varepsilon_{zz} &= \epsilon_{33} \quad \gamma_{\theta z} = 2\varepsilon_{\theta z} = \epsilon_{23} \end{aligned}$$

we have that, **considering only the linear terms**:

$$
\begin{aligned}
\varepsilon_{xx} &= u_{,x} \\
\varepsilon_{\theta\theta} &= \frac{v_{,\theta}}{R(x,z)} + \frac{u\sin\alpha}{R(x,z)} + \frac{w\cos\alpha}{R(x,z)} \\
\varepsilon_{zz} &= w_{,z} \\
\gamma_{x\theta} &= \frac{u_{,\theta}}{R(x,z)} + v_{,x} - \frac{v\sin\alpha}{R(x,z)} \\
\gamma_{xz} &= w_{,x} + u_{,z} \\
\gamma_{\theta z} &= \frac{w_{,\theta}}{R(x,z)} + v_{,z} - \frac{v\cos\alpha}{R(x,z)}
\end{aligned}
\tag{2.3}
$$

The $\sin\alpha$ and $\cos\alpha$ terms represent the coupling between in-plane and out-of-plane displacements caused by the surface curvature and its slope.

2.5 3D kinematic equations for spherical shells

Figure 11 shows the local and global coordinates of a spherical shell.

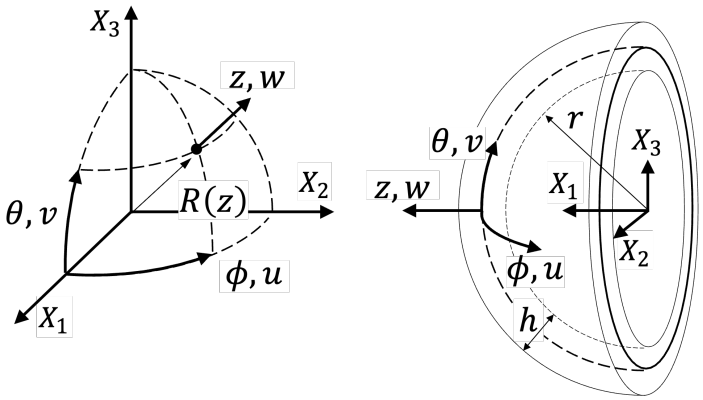

Figure 11: Spherical shell domain.

from where the following geometric relations can be derived:

$$
\begin{aligned}
x_1 = \phi \quad X_1 &= R(z)\cos\phi\cos\theta \\
x_2 = \theta \quad X_2 &= R(z)\sin\phi\cos\theta \\
x_3 = z \quad X_3 &= R(z)\sin\theta \\
R(z) &= r + z
\end{aligned}
$$

where ϕ is the longitude, θ the latitude, and the radius R is a function of the third coordinate z. Defining:

$$
\begin{aligned}
\varepsilon_{\phi\phi} = \epsilon_{11} \quad \gamma_{\phi\theta} &= 2\varepsilon_{\phi\theta} = \epsilon_{12} \\
\varepsilon_{\theta\theta} = \epsilon_{22} \quad \gamma_{\phi z} &= 2\varepsilon_{\phi z} = \epsilon_{13} \\
\varepsilon_{zz} = \epsilon_{33} \quad \gamma_{\theta z} &= 2\varepsilon_{\theta z} = \epsilon_{23}
\end{aligned}
$$

we have that, **considering only the linear terms**:

$$\begin{aligned}
\varepsilon_{\phi\phi} &= \frac{1}{R(z)}\left(\frac{u_{,\phi}}{\cos\theta} + w - v\tan\theta\right) \\
\varepsilon_{\theta\theta} &= \frac{1}{R(z)}(v_{,\theta} + w) \\
\varepsilon_{zz} &= w_{,z} \\
\gamma_{\phi\theta} &= \frac{1}{R(z)}\left(u_{,\theta} + \frac{v_{,\phi}}{\cos\theta} + u\tan\theta\right) \\
\gamma_{\phi z} &= \frac{1}{R(z)}\left(\frac{w_{,\phi}}{\cos\theta} - u\right) + u_{,z} \\
\gamma_{\theta z} &= \frac{1}{R(z)}(w_{,\theta} - v) + v_{,z}
\end{aligned} \tag{2.4}$$

The $1/\cos\theta$ and $\tan\theta$ terms arise from the curvature of the spherical surface, representing how the differential arc length changes with latitude. The presence of w (radial displacement) in both $\varepsilon_{\phi\phi}$ and $\varepsilon_{\theta\theta}$ is characteristic of shell theories where normal expansion or contraction directly contributes to the in-plane strains.

2.6 Equivalent single-layer theories

When analyzing structures, full discretization over the thickness using 3D kinematics presents several significant challenges:

- **Mesh aspect-ratio issues**: 3 to 5 first-order elements are typically needed through the thickness to capture correct bending behavior, leading to heavily distorted elements in thin structures.
- **Poor conditioning of stiffness matrix**: The conditioning scales with Eh^2 for bending and Et for membrane actions, leading to numerical instabilities.
- **Computational expense**: There is a remarkably high computational cost for laminated composite materials that feature multiple layers.
- **Boundary conditions**: Application of simply supported boundary conditions in analytical or semi-analytical models becomes highly complex.

Consequently, for thin-walled structures, utilizing strictly 3D approaches is inefficient because no prior knowledge about the deformation kinematics is embedded into the strain-displacement relations.

2.6.1 Typical Kinematic Theories Applied for Composite Plates

Most of the analyses performed on composite plates are based on one of the following approaches (Reddy, 2003):

- **Equivalent single-layer (ESL) theories (2-D)**
- Classical laminated plate theory
- Shear deformation laminated plate theories
- **Three-dimensional elasticity theory (3-D)**
- Traditional 3-D elasticity formulations
- **Layer-wise theories**

Among the ESL theories, the **First-order Shear Deformation Theory (FSDT)**, especially when including transverse extensibility ($\varepsilon_{zz} \neq 0$), provides the best compromise solution between accuracy, economy, and simplicity.

2.6.2 Equivalent Single-Layer for Shells: Mathematical Illustration

To enable ESL kinematics, the 3D domain integration must be reduced to a 2D domain integration, as illustrated in Figure 12 (Castro, 2015).

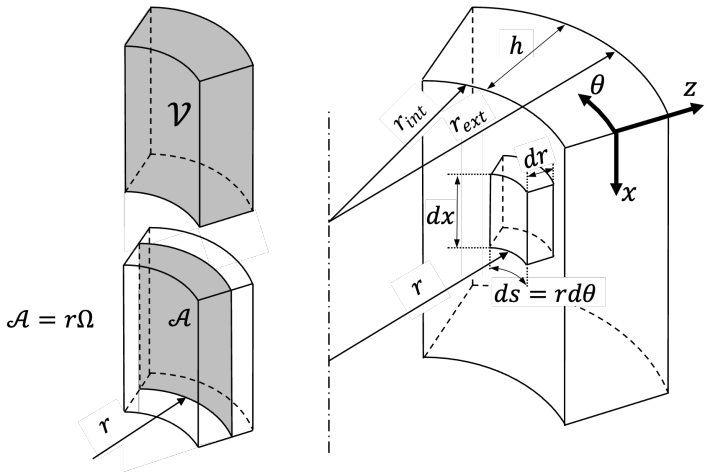

Figure 12: Shallow shell assumption $r >> h$ (Castro, 2015).

Given a function $f(x, \theta, z)$, its integral over the 3-D domain $\mathcal{V}$ can be expressed as (Castro, 2015):

$$\int_{\mathcal{V}} f(x,\theta,z)dV = \int_{r_{int}}^{r_{ext}} \int_{\Omega} f(x,\theta,z)R(x,z)d\Omega dr$$

Using substitutions based on cylindrical shell geometry:

- $d\Omega = d\theta dz$
- $R(x, z) = r + z$
- $dA = rd\Omega$
- $dr = dz$

The integral becomes:

$$\int_{\mathcal{V}} f(x,\theta,z)dV = \int_{-\frac{h}{2}}^{\frac{h}{2}} \int_{\mathcal{A}} f(x,\theta,z)(r+z)\frac{dA}{R(x,z)}dz = \int_{-\frac{h}{2}}^{\frac{h}{2}} \int_{\mathcal{A}} f(x,\theta,z)\left(1+\frac{z}{r}\right)dAdz$$

2.6.3 Applying the Shallow Shell Assumption

Applying the shallow shell theory assumption, where the radius is much larger than the thickness ($r \gg z$), results in:

$$\left(1+\frac{z}{r}\right) \approx 1$$

$$(r+z) \approx r$$

This simplification reduces the previous integral to:

$$\int_{\mathcal{V}} f(x,\theta,z)dV = \int_{-\frac{h}{2}}^{\frac{h}{2}} \int_{\mathcal{A}} f(x,\theta,z)d\mathcal{A}dz = \int_{z=-\frac{h}{2}}^{\frac{h}{2}} \int_{s=0}^{s=2\pi r} \int_{x=0}^{x=L} f(x,\theta,z)dxdsdz$$

This final equation forms the basis for reducing the 3-D domain to a 2-D domain, paving the way to integrate ESL kinematics efficiently.

2.6.4 Comparing the Main Equivalent Single-Layer (ESL) Theories

The main ESL theories make specific assumptions regarding the displacement field (u, v, w) through the thickness coordinate z.

2.6.5 Classical Laminated Plate Theory (CLPT)

The simplest of the ESL theories is the Classical Laminated Plate Theory (CLPT) which is an extension of the Classical Plate Theory to composite laminates (Reddy, 2003), where the Kirchhoff hypotheses hold (Reddy, 2003):

- Transverse normals remain straight after deformation;
- Transverse normals do not experience elongation ($\varepsilon_{zz} = 0$);
- The transverse normals rotate so that they remain perpendicular to the mid-surface after deformation (no transverse shear takes place, i.e. $\gamma_{yz} = \gamma_{xz} = 0$), leading to $\phi_x = -\frac{\partial w}{\partial x}$, illustrated in Figure 13.

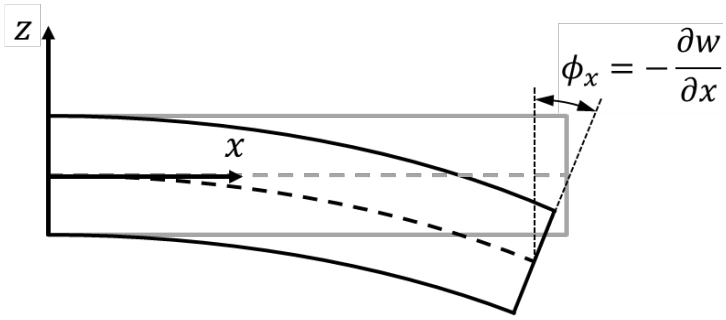

Figure 13: CLPT kinematics (Castro, 2015).

The displacement field using the CLPT (Castro, 2015) can be described by Eq. (2.5):

$$\begin{aligned} u(x,y,z) &= u_0(x,y) - z w_{,x}(x,y) \\ v(x,y,z) &= v_0(x,y) - z w_{,y}(x,y) \\ w(x,y,z) &= w_0(x,y) \end{aligned} \tag{2.5}$$

For convenience, it is customary to omit the subscript ``0'' from the mid-surface displacements, which should be clear from the context.

2.6.6 First-order Shear Deformation Theory (FSDT)

Also known as Reissner-Mindlin theory, the FSDT is the vastly most used ESL theory within finite element codes. Its popularity comes from fact that the rotations being decoupled from the deflections, enabling straightforward and compatible linear interpolation of displacements and rotations within different finite element formulations. The main kinematic features of the FSDT are:

- Rotations disconnected from normal displacements $\phi_x(x,y) \neq -w_{,x}(x,y)$.

- Transverse normals do not experience elongation ($\varepsilon_{zz} = 0$).
- Transverse shear strains γ_{xz} and γ_{yz} are constant in z. Therefore, **shear correction factors are needed**.

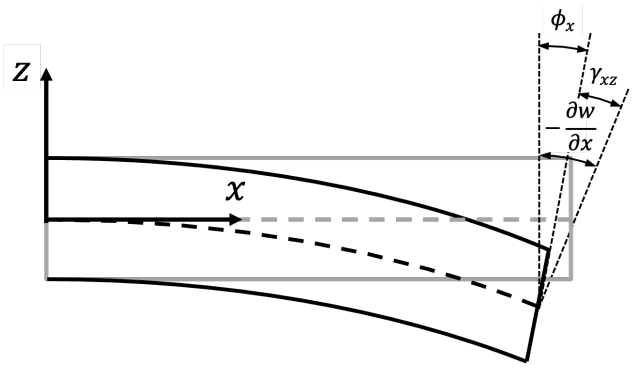

Figure 14: FSDT kinematics (Castro, 2015).

The displacement field using the FSDT (Castro, 2015) can be described by Eq. (2.6):

$$\begin{aligned} u(x,y,z) &= u_0(x,y) + z\phi_x(x,y) \\ v(x,y,z) &= v_0(x,y) + z\phi_y(x,y) \\ w(x,y,z) &= w(x,y) \end{aligned} \tag{2.6}$$

Again, for convenience, it is customary to omit the subscript ``0'' from the mid-surface displacements, which should be clear from the context. Figure 15 (Castro, 2015) visually compares the CLPT and FSDT kinematics.

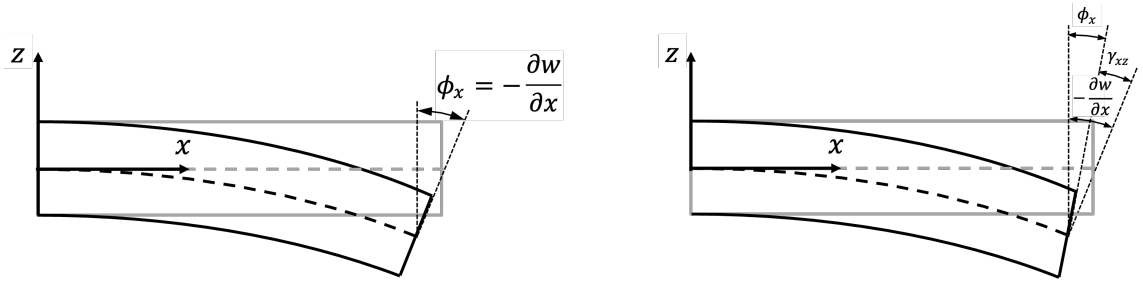

Figure 15: Kinematic comparison between CLPT and FSDT (Castro, 2015).

2.6.7 Third-order Shear Deformation Theory (TSDT)

Reddy proposed a third-order shear deformation theory that results in a second-order interpolation of the transverse shear strains (Reddy, 2003), which has the following kinematic features:

- Rotations disconnected from normal displacements $\phi_x(x,y) \neq -w_{,x}(x,y)$.
- Transverse normals do not experience elongation ($\varepsilon_{zz} = 0$).
- Consistent transverse shear strains $\gamma_{xz}(x,y,z)$ and $\gamma_{yz}(x,y,z)$, such that **shear correction factors are not needed**.

A general third-order shear deformation theory would have 9 unknown field variables, as shown below:

$$\begin{aligned} u(x,y,z) &= u_0(x,y) + z\phi_x(x,y) + z^2\theta_x(x,y) + z^3\lambda_x(x,y) \\ v(x,y,z) &= v_0(x,y) + z\phi_y(x,y) + z^2\theta_y(x,y) + z^3\lambda_y(x,y) \\ w(x,y,z) &= w_0(x,y) \end{aligned}$$

Reddy proposed, already in 1984, to impose 4 traction-free boundary conditions, on the bottom and top faces of the laminate:

$$\tau_{xz}\left(x,y,\pm\frac{h}{2}\right) = 0 \qquad \tau_{yz}\left(x,y,\pm\frac{h}{2}\right) = 0$$

which then result in the following kinematic relation with 5 unknown field variables:

$$\begin{aligned} u(x,y,z) &= u_0(x,y) + z\phi_x(x,y) - \frac{4}{3h^2}z^3\big(\phi_x(x,y) + w_{,x}(x,y)\big) \\ v(x,y,z) &= v_0(x,y) + z\phi_y(x,y) - \frac{4}{3h^2}z^3\big(\phi_y(x,y) + w_{,y}(x,y)\big) \\ w(x,y,z) &= w(x,y) \end{aligned} \tag{2.7}$$

Again, for convenience, it is customary to omit the subscript ``0'' from the mid-surface displacements, which should be clear from the context. Figure 16 (Reddy, 2003) visually compares the CLPT, FSDT and TSDT kinematics.

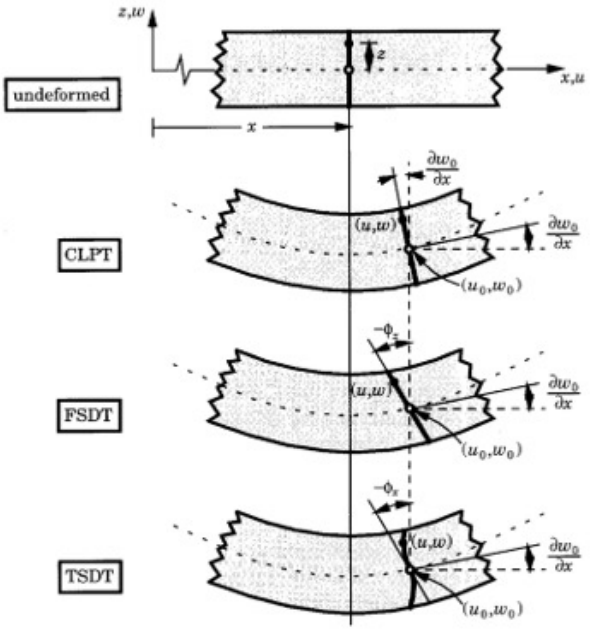

Figure 16: Kinematic comparison between CLPT, FSDT and TSDT (Reddy, 2003).

2.7 ESL equations for plates

2.7.1 CLPT for plates

For a plate, the displacement field can be approximated using the CLPT using the definitions of Eq. (2.5) into Eq. (2.1) (Castro, 2015)):

$$
\begin{aligned}
\varepsilon_{xx} &= u_{,x} - zw_{,xx} + \frac{1}{2}\left((zw_{,xx} - u_{,x})^2 + (zw_{,xy} - v_{,x})^2 + w_{,x}^2\right) \\
\varepsilon_{yy} &= v_{,y} - zw_{,yy} + \frac{1}{2}\left((zw_{,xy} - u_{,y})^2 + (zw_{,yy} - v_{,y})^2 + w_{,y}^2\right) \\
\varepsilon_{zz} &= 0 \text{ (thickness remains constant during bending)} \\
\gamma_{xy} &= u_{,y} + v_{,x} - 2zw_{,xy} + (zw_{,xx} - u_{,x})(zw_{,xy} - u_{,y}) + (zw_{,xy} - v_{,x})(zw_{,yy} - v_{,y}) + w_{,x}w_{,y} \\
\gamma_{xz} &= 0 \\
\gamma_{yz} &= 0
\end{aligned}
\tag{2.8}
$$

Using van Kármán kinematics, many of the nonlinear terms are simplified (Castro, 2015):

$$
\begin{aligned}
\varepsilon_{xx} &= u_{,x} - zw_{,xx} + \frac{1}{2}w_{,x}^2 \\
\varepsilon_{yy} &= v_{,y} - zw_{,yy} + \frac{1}{2}w_{,y}^2 \\
\varepsilon_{zz} &= 0 \text{ (thickness remains constant during bending)} \\
\gamma_{xy} &= u_{,y} + v_{,x} - 2zw_{,xy} + w_{,x}w_{,y} \\
\gamma_{xz} &= 0 \\
\gamma_{yz} &= 0
\end{aligned}
\tag{2.9}
$$

2.7.2 FSDT for plates

For a plate, the displacement field can be approximated using the FSDT using the definitions of Eq. (2.6) in (2.1) (Castro, 2015)):

$$
\begin{aligned}
\varepsilon_{xx} &= u_{,x} + z\phi_{x,x} + \frac{1}{2}\left((z\phi_{x,x} + u_{,x})^2 + (z\phi_{y,x} + v_{,x})^2 + w_{,x}^2\right) \\
\varepsilon_{yy} &= v_{,y} + z\phi_{y,y} + \frac{1}{2}\left((z\phi_{x,y} + u_{,y})^2 + (z\phi_{y,y} + v_{,y})^2 + w_{,y}^2\right) \\
\varepsilon_{zz} &= 0 \text{ (thickness remains constant during bending)} \\
\gamma_{xy} &= u_{,y} + v_{,x} + z\phi_{x,y} + z\phi_{y,x} + (z\phi_{x,x} + u_{,x})(z\phi_{x,y} + u_{,y}) + (z\phi_{y,x} + v_{,x})(z\phi_{y,y} + v_{,y}) + w_{,x}w_{,y} \\
\gamma_{xz} &= \phi_x + w_{,x} + (z\phi_{x,x} + u_{,x})\phi_x + (z\phi_{y,x} + v_{,x})\phi_y \\
\gamma_{yz} &= \phi_y + w_{,y} + (z\phi_{x,y} + u_{,y})\phi_x + (z\phi_{y,y} + v_{,y})\phi_y
\end{aligned}
\tag{2.10}
$$

Using van Kármán Kinematics:

$$
\begin{aligned}
\varepsilon_{xx} &= u_{,x} + z\phi_{x,x} + \frac{1}{2}w_{,x}^2 \\
\varepsilon_{yy} &= v_{,y} + z\phi_{y,y} + \frac{1}{2}w_{,y}^2 \\
\varepsilon_{zz} &= 0 \text{ (thickness remains constant during bending)} \\
\gamma_{xy} &= u_{,y} + v_{,x} + z\phi_{x,y} + z\phi_{y,x} + w_{,x}w_{,y} \\
\gamma_{xz} &= \phi_x + w_{,x} \\
\gamma_{yz} &= \phi_y + w_{,y}
\end{aligned}
\tag{2.11}
$$

It is usual to separate the terms multiplying ``z'' in the form of Eq. (2.12):

$$\boldsymbol{\varepsilon} = \begin{Bmatrix} \varepsilon_{xx} \\ \varepsilon_{yy} \\ 2\varepsilon_{xy} \end{Bmatrix} = \begin{Bmatrix} u_{0,x} \\ v_{0,y} \\ u_{0,y} + v_{0,x} \end{Bmatrix} + z \begin{Bmatrix} \phi_{x,x} \\ \phi_{y,y} \\ \phi_{x,y} + \phi_{y,x} \end{Bmatrix} \tag{2.12}$$
$$\boldsymbol{\gamma} = \begin{Bmatrix} 2\varepsilon_{yz} \\ 2\varepsilon_{xz} \end{Bmatrix} = \begin{Bmatrix} \gamma_{yz} \\ \gamma_{xz} \end{Bmatrix} = \begin{Bmatrix} w_{,y} + \phi_y \\ w_{,x} + \phi_x \end{Bmatrix}$$

or, using Voigt's notation:

$$\boldsymbol{\varepsilon} = \boldsymbol{\varepsilon}^{(0)} + z\boldsymbol{\varepsilon}^{(1)}$$
$$\boldsymbol{\gamma} = \boldsymbol{\gamma}^{(0)}$$

Note that all relations presented for the FSDT represent a more general case than the CLPT, and can be directly converted to the latter by doing:

$$\phi_x = -w_{,x}$$
$$\phi_y = -w_{,y}$$
$$\gamma_{xz} = 0$$
$$\gamma_{yz} = 0$$

2.7.3 TSDT for plates

For a plate, the displacement field can be approximated using the TSDT using the definitions of Eq. (2.7) in (2.1) (Castro, 2025). In Eq. (2.13), only the linear terms are shown:

$$\varepsilon_{xx} = u_{,x} + \frac{1}{2}w_{,x}^2 + z\phi_{x,x} + z^3\left(-\frac{4}{3h^2}\right)(\phi_{x,x} + w_{,xx})$$
$$\varepsilon_{yy} = v_{,y} + \frac{1}{2}w_{,y}^2 + z\phi_{y,y} + z^3\left(-\frac{4}{3h^2}\right)(\phi_{y,y} + w_{,yy})$$
$$\gamma_{xy} = u_{,y} + v_{,x} + w_{,x}w_{,y} + z\phi_{x,y} + z\phi_{y,x} + z^3\left(-\frac{4}{3h^2}\right)(\phi_{x,y} + \phi_{y,x} + 2w_{,xy}) \tag{2.13}$$
$$\gamma_{xz} = \phi_x + w_{,x} + z^2\left(-\frac{4}{h^2}\right)(\phi_x + w_{,x})$$
$$\gamma_{yz} = \phi_y + w_{,y} + z^2\left(-\frac{4}{h^2}\right)(\phi_y + w_{,y})$$

or, using Voigt's notation:

$$\boldsymbol{\varepsilon} = \begin{Bmatrix} \varepsilon_{xx} \\ \varepsilon_{yy} \\ 2\varepsilon_{xy} \end{Bmatrix} = \begin{Bmatrix} u_{0,x} \\ v_{0,y} \\ u_{0,y} + v_{0,x} \end{Bmatrix} + z \begin{Bmatrix} \phi_{x,x} \\ \phi_{y,y} \\ \phi_{x,y} + \phi_{y,x} \end{Bmatrix} + z^3\left(-\frac{4}{3h^2}\right) \begin{Bmatrix} \phi_{x,x} + w_{,xx} \\ \phi_{y,y} + w_{,yy} \\ \phi_{x,y} + \phi_{y,x} + 2w_{,xy} \end{Bmatrix}$$
$$\boldsymbol{\gamma} = \begin{Bmatrix} 2\varepsilon_{yz} \\ 2\varepsilon_{xz} \end{Bmatrix} = \begin{Bmatrix} \gamma_{yz} \\ \gamma_{xz} \end{Bmatrix} = \begin{Bmatrix} w_{,y} + \phi_y \\ w_{,x} + \phi_x \end{Bmatrix} + z^2\left(-\frac{4}{h^2}\right) \begin{Bmatrix} w_{,y} + \phi_y \\ w_{,x} + \phi_x \end{Bmatrix}$$

which becomes:

$$\boldsymbol{\varepsilon} = \boldsymbol{\varepsilon}^{(0)} + z\boldsymbol{\varepsilon}^{(1)} + z^3\boldsymbol{\varepsilon}^{(3)}$$
$$\boldsymbol{\gamma} = \boldsymbol{\gamma}^{(0)} + z^2\boldsymbol{\gamma}^{(2)}$$

Again, the subscript ``0'' for the mid-surface expressions is usually omitted.

3 Static analysis of plates

3.1 Deflection of a plate using 3D elasticity

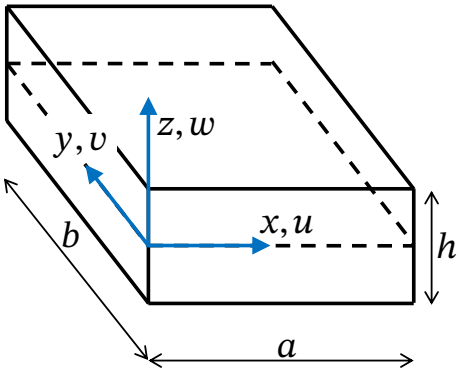

Figure 17: Plate with a point load at the centre.

Using three-dimensional (3D) elasticity, the strain-displacement equations including van Kármán non-linear terms can be written as:

$$\begin{aligned}
\varepsilon_{xx} &= u_{,x} + \frac{1}{2} w_{,x}^2 \\
\varepsilon_{yy} &= v_{,y} + \frac{1}{2} w_{,y}^2 \\
\varepsilon_{zz} &= w_{,z} + \frac{1}{2} w_{,z}^2 \\
\gamma_{xy} &= u_{,y} + v_{,x} + w_{,x} w_{,y} \\
\gamma_{xz} &= u_{,z} + w_{,x} + w_{,x} w_{,z} \\
\gamma_{yz} &= v_{,z} + w_{,y} + w_{,y} w_{,z}
\end{aligned}$$

The displacement field consists of:

$$\begin{aligned}
u(x, y, z) \\
v(x, y, z) \\
w(x, y, z)
\end{aligned}$$

Using the Ritz method:

$$\begin{aligned}
u(x, y, z) &= \boldsymbol{S}^u \bar{\boldsymbol{u}} \\
v(x, y, z) &= \boldsymbol{S}^v \bar{\boldsymbol{u}} \\
w(x, y, z) &= \boldsymbol{S}^w \bar{\boldsymbol{u}}
\end{aligned}$$

The linear strains become:

$$\begin{aligned}
\varepsilon_{xx} &= \boldsymbol{S}^u_{,x} \bar{\boldsymbol{u}} \\
\varepsilon_{yy} &= \boldsymbol{S}^v_{,y} \bar{\boldsymbol{u}} \\
\gamma_{xy} &= \boldsymbol{S}^u_{,y} + \boldsymbol{S}^v_{,x} \bar{\boldsymbol{u}}
\end{aligned}$$

and:

$$\boldsymbol{\varepsilon} = \boldsymbol{B}\bar{\boldsymbol{u}}$$

The stiffness matrix becomes, using the 3D constitutive matrix $\boldsymbol{C}$:

$$\boldsymbol{K} = \iiint_{x,y,z} \boldsymbol{B}^\top \boldsymbol{C}\boldsymbol{B} dx dy dz$$

The external force vector in this example includes only a point load P at the center top surface of the plate:

$$\boldsymbol{F}_{ext} = P\boldsymbol{S}^w \Big|_{\substack{x=a/2 \\ y=b/2 \\ z=+h/2}}$$

Solution for the unknown Ritz coefficients:

$$\bar{\boldsymbol{u}} = \boldsymbol{K}^{-1}\boldsymbol{F}_{ext}$$

And the strain recovery becomes:

$$\boldsymbol{\varepsilon} = \boldsymbol{B}\bar{\boldsymbol{u}}$$

An example of the 3D deflection of a plate can be seen in this notebook.

3.2 Deflection of a plate using CLPT

The kinematic (strain-displacement) equations using the clasical laminated plate theory (CLPT), including van Kármán non-linear are:

$$\begin{aligned}
\varepsilon_{xx} &= u_{,x} - z w_{,xx} + \frac{1}{2} w_{,x}^2 \\
\varepsilon_{yy} &= v_{,y} - z w_{,yy} + \frac{1}{2} w_{,y}^2 \\
\gamma_{xy} &= u_{,y} + v_{,x} - 2z w_{,xy} + w_{,x} w_{,y}
\end{aligned}$$

In the CLPT, the rotation of the plate is assumed constant through the thickness and field approximation (CLPT kinematics):

$$\begin{aligned}
u(x,y,z) &= u_0(x,y) - z w_{,x}(x,y) \\
v(x,y,z) &= v_0(x,y) - z w_{,y}(x,y) \\
w(x,y,z) &= w_0(x,y)
\end{aligned}$$

Using the Ritz method:

$$\begin{aligned}
u(x,y,z) &= (\boldsymbol{S}^u - z\boldsymbol{S}^w_{,x})\bar{\boldsymbol{u}} \\
v(x,y,z) &= (\boldsymbol{S}^v - z\boldsymbol{S}^w_{,y})\bar{\boldsymbol{u}} \\
w(x,y) &= \boldsymbol{S}^w \bar{\boldsymbol{u}}
\end{aligned}$$

The linear strains then become:

$$\begin{aligned}
\varepsilon_{xx} &= (\boldsymbol{S}^u_{,x} - z\boldsymbol{S}^w_{,xx})\bar{\boldsymbol{u}} \\
\varepsilon_{yy} &= (\boldsymbol{S}^v_{,y} - z\boldsymbol{S}^w_{,yy})\bar{\boldsymbol{u}} \\
\gamma_{xy} &= (\boldsymbol{S}^u_{,y} + \boldsymbol{S}^v_{,x} - 2z\boldsymbol{S}^w_{,xy})\bar{\boldsymbol{u}}
\end{aligned}$$

Matrix separation into membrane ($\boldsymbol{B}_m$) and bending ($\boldsymbol{B}_b$) operators:

$$\boldsymbol{\varepsilon} = \begin{Bmatrix} \varepsilon_{xx} \\ \varepsilon_{yy} \\ \gamma_{xy} \end{Bmatrix} = \left(\begin{bmatrix} \boldsymbol{S}^u_{,x} \\ \boldsymbol{S}^v_{,y} \\ \boldsymbol{S}^u_{,y} + \boldsymbol{S}^v_{,x} \end{bmatrix} + z \begin{bmatrix} -\boldsymbol{S}^w_{,xx} \\ -\boldsymbol{S}^w_{,yy} \\ -2\boldsymbol{S}^w_{,xy} \end{bmatrix} \right) \bar{\boldsymbol{u}}$$

$$\boldsymbol{\varepsilon} = (\boldsymbol{B}_m + z\boldsymbol{B}_b)\bar{\boldsymbol{u}}$$

The stiffness matrix becomes, using the laminate constitutive matrices $\boldsymbol{A}, \boldsymbol{B}, \boldsymbol{D}$:

$$\boldsymbol{K} = \iint_{x,y} \left(\boldsymbol{B}_m^\top \boldsymbol{A} \boldsymbol{B}_m \right) + \left(\boldsymbol{B}_b^\top \boldsymbol{D} \boldsymbol{B}_b \right) + \left(\boldsymbol{B}_m^\top \boldsymbol{B} \boldsymbol{B}_b \right) + \left(\boldsymbol{B}_b^\top \boldsymbol{B} \boldsymbol{B}_m \right) dxdy$$

External force vector (point load P at the midplane):

$$\boldsymbol{F}_{ext} = P\boldsymbol{S}^w \Big|_{\substack{x = a/2 \\ y = b/2}}$$

Solution for unknown coefficients:

$$\bar{\boldsymbol{u}} = \boldsymbol{K}^{-1} \boldsymbol{F}_{ext}$$

An example of the deflection of a plate using the CLPT can be seen in this notebook.

3.3 Deflection of a plate using FSDT

For the first-order shear deformation theory (FSDT), the rotations of the displacement field approximation are decoupled from the gradients of w by creating two independent field variables ϕ_x and ϕ_y:

$$\begin{aligned} u(x,y,z) &= u_0(x,y) + z\phi_x(x,y) \\ v(x,y,z) &= v_0(x,y) + z\phi_y(x,y) \\ w(x,y,z) &= w(x,y) \end{aligned}$$

Using the Ritz method:

$$\begin{aligned} u(x,y,z) &= (\boldsymbol{S}^u + z\boldsymbol{S}^{\phi_x})\bar{\boldsymbol{u}} \\ v(x,y,z) &= (\boldsymbol{S}^v + z\boldsymbol{S}^{\phi_y})\bar{\boldsymbol{u}} \\ w(x,y) &= \boldsymbol{S}^w \bar{\boldsymbol{u}} \end{aligned}$$

The kinematic (strain-displacement) equations for the FSDT, including van Kármán non-linear are:

$$\begin{aligned} \varepsilon_{xx} &= u_{,x} + z\phi_{x,x} + \frac{1}{2} w_{,x}^2 \\ \varepsilon_{yy} &= v_{,y} + z\phi_{y,y} + \frac{1}{2} w_{,y}^2 \\ \gamma_{xy} &= u_{,y} + v_{,x} + z\phi_{x,y} + z\phi_{y,x} + w_{,x} w_{,y} \\ \gamma_{xz} &= \phi_x + w_{,x} \\ \gamma_{yz} &= \phi_y + w_{,y} \end{aligned}$$

The linear strains terms are:

$$
\begin{aligned}
\varepsilon_{xx} &= (\boldsymbol{S}^{u}_{,x} + z\boldsymbol{S}^{\phi_x}_{,x})\bar{\boldsymbol{u}} \\
\varepsilon_{yy} &= (\boldsymbol{S}^{v}_{,y} + z\boldsymbol{S}^{\phi_y}_{,y})\bar{\boldsymbol{u}} \\
\gamma_{xy} &= (\boldsymbol{S}^{u}_{,y} + \boldsymbol{S}^{v}_{,x} + z\boldsymbol{S}^{\phi_x}_{,y} + z\boldsymbol{S}^{\phi_y}_{,x})\bar{\boldsymbol{u}} \\
\gamma_{yz} &= (\boldsymbol{S}^{\phi_y} + \boldsymbol{S}^{w}_{,y})\bar{\boldsymbol{u}} \\
\gamma_{xz} &= (\boldsymbol{S}^{\phi_x} + \boldsymbol{S}^{w}_{,x})\bar{\boldsymbol{u}}
\end{aligned}
$$

Stress resultant operator definitions:

$$
\begin{aligned}
\boldsymbol{B}^N &= \boldsymbol{A}\begin{Bmatrix} \boldsymbol{B}^{\varepsilon^{(0)}_{xx}} \\ \boldsymbol{B}^{\varepsilon^{(0)}_{yy}} \\ \boldsymbol{B}^{\gamma^{(0)}_{xy}} \end{Bmatrix} + \boldsymbol{B}\begin{Bmatrix} \boldsymbol{B}^{\varepsilon^{(1)}_{xx}} \\ \boldsymbol{B}^{\varepsilon^{(1)}_{yy}} \\ \boldsymbol{B}^{\gamma^{(1)}_{xy}} \end{Bmatrix} \\
\boldsymbol{B}^M &= \boldsymbol{B}\begin{Bmatrix} \boldsymbol{B}^{\varepsilon^{(0)}_{xx}} \\ \boldsymbol{B}^{\varepsilon^{(0)}_{yy}} \\ \boldsymbol{B}^{\gamma^{(0)}_{xy}} \end{Bmatrix} + \boldsymbol{D}\begin{Bmatrix} \boldsymbol{B}^{\varepsilon^{(1)}_{xx}} \\ \boldsymbol{B}^{\varepsilon^{(1)}_{yy}} \\ \boldsymbol{B}^{\gamma^{(1)}_{xy}} \end{Bmatrix} \\
\boldsymbol{B}^Q &= \boldsymbol{A}\begin{Bmatrix} \boldsymbol{B}^{\gamma^{(0)}_{yz}} \\ \boldsymbol{B}^{\gamma^{(0)}_{xz}} \end{Bmatrix}
\end{aligned}
$$

For the FSDT, the variation of the strain energy is:

$$
\delta U = \iint_{xy} \left(\boldsymbol{N}^\top \begin{Bmatrix} \delta\varepsilon^{(0)}_{xx} \\ \delta\varepsilon^{(0)}_{yy} \\ \delta\gamma^{(0)}_{xy} \end{Bmatrix} + \boldsymbol{M}^\top \begin{Bmatrix} \delta\varepsilon^{(1)}_{xx} \\ \delta\varepsilon^{(1)}_{yy} \\ \delta\gamma^{(1)}_{xy} \end{Bmatrix} + \boldsymbol{Q}^\top \begin{Bmatrix} \delta\gamma^{(0)}_{yz} \\ \delta\gamma^{(0)}_{xz} \end{Bmatrix} \right) dxdy
$$

Such that the stiffness matrix becomes, using the laminate constitutive matrices $\boldsymbol{A}, \boldsymbol{B}, \boldsymbol{D}$:

$$
\boldsymbol{K} = \iint_{xy} \left(\boldsymbol{B}^{N\top} \begin{Bmatrix} \boldsymbol{B}^{\varepsilon^{(0)}_{xx}} \\ \boldsymbol{B}^{\varepsilon^{(0)}_{yy}} \\ \boldsymbol{B}^{\gamma^{(0)}_{xy}} \end{Bmatrix} + \boldsymbol{B}^{M\top} \begin{Bmatrix} \boldsymbol{B}^{\varepsilon^{(1)}_{xx}} \\ \boldsymbol{B}^{\varepsilon^{(1)}_{yy}} \\ \boldsymbol{B}^{\gamma^{(1)}_{xy}} \end{Bmatrix} + \boldsymbol{B}^{Q\top} \begin{Bmatrix} \boldsymbol{B}^{\gamma^{(0)}_{yz}} \\ \boldsymbol{B}^{\gamma^{(0)}_{xz}} \end{Bmatrix} \right) dxdy
$$

The external force vector is then defined as:

$$
\boldsymbol{F}_{ext} = P\boldsymbol{S}^{w}\Big|_{\substack{x = a/2 \\ y = b/2}}
$$

Which can be solved for the Ritz coefficients with:

$$
\bar{\boldsymbol{u}} = \boldsymbol{K}^{-1}\boldsymbol{F}_{ext}
$$

An example of the deflection of a plate using the FSDT can be seen in this notebook.

3.4 Deflection of a plate using the TSDT

The third-order shear deformation theory enforces zero transverse shear stresses and strains at the plate faces, $z = -h/2$ and $z = +h/2$, leading to additional 4 equations that enable a third-order interpolation of displacements through the thickness that results in a consistent second-order interpolation of transverse strains and stresses (Reddy, 2003). The following displacement field representation was proposed by Reddy:

$$
\begin{aligned}
u(x,y,z) &= u_0(x,y) + z\phi_x(x,y) - \frac{4}{3h^2}z^3\left(\phi_x(x,y) + w_{,x}(x,y)\right)\\
v(x,y,z) &= v_0(x,y) + z\phi_y(x,y) - \frac{4}{3h^2}z^3\left(\phi_y(x,y) + w_{,y}(x,y)\right)\\
w(x,y,z) &= w(x,y)
\end{aligned}
$$

Using the Ritz method:

$$
\begin{aligned}
u(x,y,z) &= \left(\boldsymbol{S}^u + z\boldsymbol{S}^{\phi_x} + z^3\left(-\frac{4}{3h^2}\right)\left(\boldsymbol{S}^{\phi_x} + \boldsymbol{S}^w_{,x}\right)\right)\bar{\boldsymbol{u}}\\
v(x,y,z) &= \left(\boldsymbol{S}^v + z\boldsymbol{S}^{\phi_y} + z^3\left(-\frac{4}{3h^2}\right)\left(\boldsymbol{S}^{\phi_y} + \boldsymbol{S}^w_{,y}\right)\right)\bar{\boldsymbol{u}}\\
w(x,y) &= \boldsymbol{S}^w\bar{\boldsymbol{u}}
\end{aligned}
$$

Strain-displacement equations, including van K'arm\an non-linear terms:

$$
\begin{aligned}
\varepsilon_{xx} &= u_{,x} + \frac{1}{2}w_{,x}^2 + z\phi_{x,x} + z^3\left(-\frac{4}{3h^2}\right)\left(\phi_{x,x} + w_{,xx}\right)\\
\varepsilon_{yy} &= v_{,y} + \frac{1}{2}w_{,y}^2 + z\phi_{y,y} + z^3\left(-\frac{4}{3h^2}\right)\left(\phi_{y,y} + w_{,yy}\right)\\
\gamma_{xy} &= u_{,y} + v_{,x} + w_{,x}w_{,y} + z\phi_{x,y} + z\phi_{y,x} + z^3\left(-\frac{4}{3h^2}\right)\left(\phi_{x,y} + \phi_{y,x} + 2w_{,xy}\right)\\
\gamma_{xz} &= \phi_x + w_{,x} + z^2\left(-\frac{4}{h^2}\right)\left(\phi_x + w_{,x}\right)\\
\gamma_{yz} &= \phi_y + w_{,y} + z^2\left(-\frac{4}{h^2}\right)\left(\phi_y + w_{,y}\right)
\end{aligned}
$$

The linear strains then become:

$$
\begin{aligned}
\varepsilon_{xx} &= \left(\boldsymbol{S}^u_{,x} + z\boldsymbol{S}^{\phi_x}_{,x} + z^3\left(-\frac{4}{3h^2}\right)\left(\boldsymbol{S}^{\phi_x}_{,x} + \boldsymbol{S}^w_{,xx}\right)\right)\bar{\boldsymbol{u}}\\
\varepsilon_{yy} &= \left(\boldsymbol{S}^v_{,y} + z\boldsymbol{S}^{\phi_y}_{,y} + z^3\left(-\frac{4}{3h^2}\right)\left(\boldsymbol{S}^{\phi_y}_{,y} + \boldsymbol{S}^w_{,yy}\right)\right)\bar{\boldsymbol{u}}\\
\gamma_{xy} &= \left(\boldsymbol{S}^u_{,y} + \boldsymbol{S}^v_{,x} + z\boldsymbol{S}^{\phi_x}_{,y} + z\boldsymbol{S}^{\phi_y}_{,x} + z^3\left(-\frac{4}{3h^2}\right)\left(\boldsymbol{S}^{\phi_x}_{,y} + \boldsymbol{S}^{\phi_y}_{,x} + 2\boldsymbol{S}^w_{,xy}\right)\right)\bar{\boldsymbol{u}}\\
\gamma_{yz} &= \left(\boldsymbol{S}^{\phi_y} + \boldsymbol{S}^w_{,y} + z^2\left(-\frac{4}{h^2}\right)\left(\boldsymbol{S}^{\phi_y} + \boldsymbol{S}^w_{,y}\right)\right)\bar{\boldsymbol{u}}\\
\gamma_{xz} &= \left(\boldsymbol{S}^{\phi_x} + \boldsymbol{S}^w_{,x} + z^2\left(-\frac{4}{h^2}\right)\left(\boldsymbol{S}^{\phi_x} + \boldsymbol{S}^w_{,x}\right)\right)\bar{\boldsymbol{u}}
\end{aligned}
$$

Stress resultant operator definitions:

$$
\begin{aligned}
\boldsymbol{B}^N &= \boldsymbol{A}\begin{Bmatrix} \boldsymbol{B}^{\varepsilon_{xx}^{(0)}} \\ \boldsymbol{B}^{\varepsilon_{yy}^{(0)}} \\ \boldsymbol{B}^{\gamma_{xy}^{(0)}} \end{Bmatrix} + \boldsymbol{B}\begin{Bmatrix} \boldsymbol{B}^{\varepsilon_{xx}^{(1)}} \\ \boldsymbol{B}^{\varepsilon_{yy}^{(1)}} \\ \boldsymbol{B}^{\gamma_{xy}^{(1)}} \end{Bmatrix} + \boldsymbol{E}\begin{Bmatrix} \boldsymbol{B}^{\varepsilon_{xx}^{(3)}} \\ \boldsymbol{B}^{\varepsilon_{yy}^{(3)}} \\ \boldsymbol{B}^{\gamma_{xy}^{(3)}} \end{Bmatrix} \\
\boldsymbol{B}^M &= \boldsymbol{B}\begin{Bmatrix} \boldsymbol{B}^{\varepsilon_{xx}^{(0)}} \\ \boldsymbol{B}^{\varepsilon_{yy}^{(0)}} \\ \boldsymbol{B}^{\gamma_{xy}^{(0)}} \end{Bmatrix} + \boldsymbol{D}\begin{Bmatrix} \boldsymbol{B}^{\varepsilon_{xx}^{(1)}} \\ \boldsymbol{B}^{\varepsilon_{yy}^{(1)}} \\ \boldsymbol{B}^{\gamma_{xy}^{(1)}} \end{Bmatrix} + \boldsymbol{F}\begin{Bmatrix} \boldsymbol{B}^{\varepsilon_{xx}^{(3)}} \\ \boldsymbol{B}^{\varepsilon_{yy}^{(3)}} \\ \boldsymbol{B}^{\gamma_{xy}^{(3)}} \end{Bmatrix} \\
\boldsymbol{B}^P &= \boldsymbol{E}\begin{Bmatrix} \boldsymbol{B}^{\varepsilon_{xx}^{(0)}} \\ \boldsymbol{B}^{\varepsilon_{yy}^{(0)}} \\ \boldsymbol{B}^{\gamma_{xy}^{(0)}} \end{Bmatrix} + \boldsymbol{F}\begin{Bmatrix} \boldsymbol{B}^{\varepsilon_{xx}^{(1)}} \\ \boldsymbol{B}^{\varepsilon_{yy}^{(1)}} \\ \boldsymbol{B}^{\gamma_{xy}^{(1)}} \end{Bmatrix} + \boldsymbol{H}\begin{Bmatrix} \boldsymbol{B}^{\varepsilon_{xx}^{(3)}} \\ \boldsymbol{B}^{\varepsilon_{yy}^{(3)}} \\ \boldsymbol{B}^{\gamma_{xy}^{(3)}} \end{Bmatrix} \\
\boldsymbol{B}^Q &= \boldsymbol{A}\begin{Bmatrix} \boldsymbol{B}^{\gamma_{yz}^{(0)}} \\ \boldsymbol{B}^{\gamma_{xz}^{(0)}} \end{Bmatrix} + \boldsymbol{D}\begin{Bmatrix} \boldsymbol{B}^{\gamma_{yz}^{(2)}} \\ \boldsymbol{B}^{\gamma_{xz}^{(2)}} \end{Bmatrix} \\
\boldsymbol{B}^R &= \boldsymbol{D}\begin{Bmatrix} \boldsymbol{B}^{\gamma_{yz}^{(0)}} \\ \boldsymbol{B}^{\gamma_{xz}^{(0)}} \end{Bmatrix} + \boldsymbol{F}\begin{Bmatrix} \boldsymbol{B}^{\gamma_{yz}^{(2)}} \\ \boldsymbol{B}^{\gamma_{xz}^{(2)}} \end{Bmatrix}
\end{aligned}
$$

For the TSDT, the variation of the strain energy is:

$$
\delta U = \iint_{xy} \left(\boldsymbol{N}^\top \begin{Bmatrix} \delta\varepsilon_{xx}^{(0)} \\ \delta\varepsilon_{yy}^{(0)} \\ \delta\gamma_{xy}^{(0)} \end{Bmatrix} + \boldsymbol{M}^\top \begin{Bmatrix} \delta\varepsilon_{xx}^{(1)} \\ \delta\varepsilon_{yy}^{(1)} \\ \delta\gamma_{xy}^{(1)} \end{Bmatrix} + \boldsymbol{P}^\top \begin{Bmatrix} \delta\varepsilon_{xx}^{(3)} \\ \delta\varepsilon_{yy}^{(3)} \\ \delta\gamma_{xy}^{(3)} \end{Bmatrix} + \boldsymbol{Q}^\top \begin{Bmatrix} \delta\gamma_{yz}^{(0)} \\ \delta\gamma_{xz}^{(0)} \end{Bmatrix} + \boldsymbol{R}^\top \begin{Bmatrix} \delta\gamma_{yz}^{(2)} \\ \delta\gamma_{xz}^{(2)} \end{Bmatrix} \right) dxdy
$$

Such that the stiffness matrix becomes, using the laminate constitutive matrices $\boldsymbol{A}, \boldsymbol{B}, \boldsymbol{D}, \boldsymbol{E}, \boldsymbol{F}, \boldsymbol{G}$:

$$
\boldsymbol{K} = \iint_{xy} \left(\boldsymbol{B}^{N\top} \begin{Bmatrix} \boldsymbol{B}^{\varepsilon_{xx}^{(0)}} \\ \boldsymbol{B}^{\varepsilon_{yy}^{(0)}} \\ \boldsymbol{B}^{\gamma_{xy}^{(0)}} \end{Bmatrix} + \boldsymbol{B}^{M\top} \begin{Bmatrix} \boldsymbol{B}^{\varepsilon_{xx}^{(1)}} \\ \boldsymbol{B}^{\varepsilon_{yy}^{(1)}} \\ \boldsymbol{B}^{\gamma_{xy}^{(1)}} \end{Bmatrix} + \boldsymbol{B}^{P\top} \begin{Bmatrix} \boldsymbol{B}^{\varepsilon_{xx}^{(3)}} \\ \boldsymbol{B}^{\varepsilon_{yy}^{(3)}} \\ \boldsymbol{B}^{\gamma_{xy}^{(3)}} \end{Bmatrix} + \boldsymbol{B}^{Q\top} \begin{Bmatrix} \boldsymbol{B}^{\gamma_{yz}^{(0)}} \\ \boldsymbol{B}^{\gamma_{xz}^{(0)}} \end{Bmatrix} + \boldsymbol{B}^{R\top} \begin{Bmatrix} \boldsymbol{B}^{\gamma_{yz}^{(2)}} \\ \boldsymbol{B}^{\gamma_{xz}^{(2)}} \end{Bmatrix} \right) dxdy
$$

External force vector:

$$
\boldsymbol{F}_{ext} = P\boldsymbol{S}^w \Big|_{\substack{x = a/2 \\ y = b/2}}
$$

Which can be solved for the Ritz coefficients:

$$
\bar{\boldsymbol{u}} = \boldsymbol{K}^{-1}\boldsymbol{F}_{ext}
$$

An example of the deflection of a plate using the TSDT can be seen in this notebook.

4 Linear buckling of plates with general boundary conditions

4.1 Geometric stiffness

4.1.1 Geometric stiffness for beams

Using the full nonlinear Green-Lagrange strain relation, the axial strain of a beam can be written as:

$$\varepsilon_{xx} = \frac{\partial u}{\partial x} + \frac{1}{2}\left[\left(\frac{\partial u}{\partial x}\right)^2 + \left(\frac{\partial v}{\partial x}\right)^2 + \left(\frac{\partial w}{\partial x}\right)^2\right] \tag{4.1}$$

The first variation becomes, using $\partial(\cdot)/\partial x = (\cdot)_{,x}$

$$\delta\varepsilon_{xx} = \delta u_{,x} + u_{,x}\delta u_{,x} + v_{,x}\delta v_{,x} + w_{,x}\delta w_{,x} \tag{4.2}$$

In terms of nodal displacements (or Ritz coefficients) $\bar{\boldsymbol{u}}$:

$$\delta\varepsilon_{xx} = \bar{\boldsymbol{B}}\delta\bar{\boldsymbol{u}} = (\boldsymbol{B}_L + \boldsymbol{B}_{NL})\delta\bar{\boldsymbol{u}} \tag{4.3}$$

with:

$$\boldsymbol{B}_L = \frac{\partial \boldsymbol{S}^u}{\partial x}\boldsymbol{B}_{NL} = \frac{\partial u}{\partial x}\frac{\partial \boldsymbol{S}^u}{\partial x} + \frac{\partial v}{\partial x}\frac{\partial \boldsymbol{S}^v}{\partial x} + \frac{\partial w}{\partial x}\frac{\partial \boldsymbol{S}^w}{\partial x} \tag{4.4}$$

The second variation becomes:

$$\delta^2\varepsilon_{xx} = \delta^2 u_{,x} + \delta u_{,x}\delta u_{,x} + u_{,x}\delta^2 u_{,x} + \delta v_{,x}\delta v_{,x} + v_{,x}\delta^2 v_{,x} + \delta w_{,x}\delta w_{,x} + w_{,x}\delta^2 w_{,x} \tag{4.5}$$

Note that $\delta^2(\cdot)_{,x} \ll \delta(\cdot)_{,x}$, leading to:

$$\delta^2\varepsilon_{xx} = \delta u_{,x}\delta u_{,x} + \delta v_{,x}\delta v_{,x} + \delta w_{,x}\delta w_{,x} \tag{4.6}$$

with $\delta^2\varepsilon_{xx}$ defined as:

$$\delta^2\varepsilon_{xx} = \delta u_{,x}\delta u_{,x} + \delta v_{,x}\delta v_{,x} + \delta w_{,x}\delta w_{,x} \tag{4.7}$$

using the finite element (or Ritz method) shape functions:

$$\delta^2\varepsilon_{xx} = \delta\bar{\boldsymbol{u}}^\top\left[\left(\frac{\partial \boldsymbol{S}^u}{\partial x}\right)^\top\left(\frac{\partial \boldsymbol{S}^u}{\partial x}\right) + \left(\frac{\partial \boldsymbol{S}^v}{\partial x}\right)^\top\left(\frac{\partial \boldsymbol{S}^v}{\partial x}\right) + \left(\frac{\partial \boldsymbol{S}^w}{\partial x}\right)^\top\left(\frac{\partial \boldsymbol{S}^w}{\partial x}\right)\right]\delta\bar{\boldsymbol{u}}$$

Then:

$$\delta\bar{\boldsymbol{u}}^\top\boldsymbol{K}_G\delta\bar{\boldsymbol{u}} = \int_\Omega \hat{\sigma}_{xx}\delta^2\varepsilon_{xx}\,d\Omega$$

$$= \delta\bar{\boldsymbol{u}}^\top\int_\Omega \hat{\sigma}_{xx}\left(\frac{\partial \boldsymbol{S}^u}{\partial x}\right)^\top\left(\frac{\partial \boldsymbol{S}^u}{\partial x}\right) + \hat{\sigma}_{xx}\left(\frac{\partial \boldsymbol{S}^v}{\partial x}\right)^\top\left(\frac{\partial \boldsymbol{S}^v}{\partial x}\right) + \hat{\sigma}_{xx}\left(\frac{\partial \boldsymbol{S}^w}{\partial x}\right)^\top\left(\frac{\partial \boldsymbol{S}^w}{\partial x}\right)d\Omega\,\delta\bar{\boldsymbol{u}}$$

$\hat{\sigma}_{xx}$ can be given or calculated from an initial nodal displacement state $\hat{\boldsymbol{u}}$ (pre-buckling of fundamental state):

$$\hat{\sigma}_{xx} = E\left(\boldsymbol{B}_L + \frac{1}{2}\boldsymbol{B}_{NL}\right)\hat{\boldsymbol{u}}$$

4.1.2 Geometric stiffness for plates

For plates, using the full nonlinear Green-Lagrange strain relation:

$$\varepsilon_{xx} = \frac{\partial u}{\partial x} + \frac{1}{2}\left[\left(\frac{\partial u}{\partial x}\right)^2 + \left(\frac{\partial v}{\partial x}\right)^2 + \left(\frac{\partial w}{\partial x}\right)^2\right]$$

$$\varepsilon_{yy} = \frac{\partial v}{\partial y} + \frac{1}{2}\left[\left(\frac{\partial u}{\partial y}\right)^2 + \left(\frac{\partial v}{\partial y}\right)^2 + \left(\frac{\partial w}{\partial y}\right)^2\right]$$

$$\gamma_{xy} = \frac{\partial u}{\partial y} + \frac{\partial v}{\partial x} + \left(\frac{\partial u}{\partial x}\frac{\partial u}{\partial y} + \frac{\partial v}{\partial x}\frac{\partial v}{\partial y} + \frac{\partial w}{\partial x}\frac{\partial w}{\partial y}\right)$$

The first variation becomes, using $\partial(\cdot)/\partial x = (\cdot)_{,x}$:

$$\begin{aligned}
\delta\varepsilon_{xx} &= \delta u_{,x} + u_{,x}\delta u_{,x} + v_{,x}\delta v_{,x} + w_{,x}\delta w_{,x} \\
\delta\varepsilon_{yy} &= \delta v_{,y} + u_{,y}\delta u_{,y} + v_{,y}\delta v_{,y} + w_{,y}\delta w_{,y} \\
\delta\gamma_{xy} &= \delta u_{,y} + \delta v_{,x} + \delta u_{,x}u_{,y} + u_{,x}\delta u_{,y} + \delta v_{,x}v_{,y} + v_{,x}\delta v_{,y} + \delta w_{,x}w_{,y} + w_{,x}\delta w_{,y}
\end{aligned}$$

The second variation becomes:

$$\begin{aligned}
\delta^2\varepsilon_{xx} &= \delta^2 u_{,x} + \delta u_{,x}\delta u_{,x} + u_{,x}\delta^2 u_{,x} + \delta v_{,x}\delta v_{,x} + v_{,x}\delta^2 v_{,x} + \delta w_{,x}\delta w_{,x} + w_{,x}\delta^2 w_{,x} \\
\delta^2\varepsilon_{yy} &= \delta^2 v_{,y} + \delta u_{,y}\delta u_{,y} + u_{,y}\delta^2 u_{,y} + \delta v_{,y}\delta v_{,y} + v_{,y}\delta^2 v_{,y} + \delta w_{,y}\delta w_{,y} + w_{,y}\delta^2 w_{,y} \\
\delta^2\gamma_{xy} &= \delta^2 u_{,y} + \delta^2 v_{,x} + \delta^2 u_{,x}u_{,y} + 2\delta u_{,x}\delta u_{,y} + u_{,x}\delta^2 u_{,y} \\
&\quad + \delta^2 v_{,x}v_{,y} + 2\delta v_{,x}\delta v_{,y} + v_{,x}\delta^2 v_{,y} + \delta^2 w_{,x}w_{,y} \\
&\quad + 2\delta w_{,x}\delta w_{,y} + w_{,x}\delta^2 w_{,y}
\end{aligned}$$

Note that $\delta^2(\cdot)_{,x} \ll \delta(\cdot)_{,x}$ and $\delta^2(\cdot)_{,y} \ll \delta(\cdot)_{,y}$, leading to:

$$\delta^2\varepsilon_{xx} = \delta u_{,x}\delta u_{,x} + \delta v_{,x}\delta v_{,x} + \delta w_{,x}\delta w_{,x} \tag{4.8}$$

$$\delta^2\varepsilon_{yy} = \delta u_{,y}\delta u_{,y} + \delta v_{,y}\delta v_{,y} + \delta w_{,y}\delta w_{,y} \tag{4.9}$$

$$\delta^2\gamma_{xy} = 2\delta u_{,x}\delta u_{,y} + 2\delta v_{,x}\delta v_{,y} + 2\delta w_{,x}\delta w_{,y} \tag{4.10}$$

with $\delta^2\boldsymbol{\varepsilon}$ defined as:

$$\delta^2\varepsilon_{xx} = \delta u_{,x}\delta u_{,x} + \delta v_{,x}\delta v_{,x} + \delta w_{,x}\delta w_{,x} \tag{4.11}$$

$$\delta^2\varepsilon_{yy} = \delta u_{,y}\delta u_{,y} + \delta v_{,y}\delta v_{,y} + \delta w_{,y}\delta w_{,y} \tag{4.12}$$

$$\delta^2\gamma_{xy} = 2\delta u_{,x}\delta u_{,y} + 2\delta v_{,x}\delta v_{,y} + 2\delta w_{,x}\delta w_{,y} \tag{4.13}$$

using finite element or Ritz shape functions:

$$\delta^2\varepsilon_{xx} = \delta\bar{\boldsymbol{u}}^\top \left[\left(\frac{\partial \boldsymbol{S}^u}{\partial x}\right)^\top \left(\frac{\partial \boldsymbol{S}^u}{\partial x}\right) + \left(\frac{\partial \boldsymbol{S}^v}{\partial x}\right)^\top \left(\frac{\partial \boldsymbol{S}^v}{\partial x}\right) + \left(\frac{\partial \boldsymbol{S}^w}{\partial x}\right)^\top \left(\frac{\partial \boldsymbol{S}^w}{\partial x}\right) \right] \delta\bar{\boldsymbol{u}} \tag{4.14}$$

$$\delta^2\varepsilon_{yy} = \delta\bar{\boldsymbol{u}}^\top \left[\left(\frac{\partial \boldsymbol{S}^u}{\partial y}\right)^\top \left(\frac{\partial \boldsymbol{S}^u}{\partial y}\right) + \left(\frac{\partial \boldsymbol{S}^v}{\partial y}\right)^\top \left(\frac{\partial \boldsymbol{S}^v}{\partial y}\right) + \left(\frac{\partial \boldsymbol{S}^w}{\partial y}\right)^\top \left(\frac{\partial \boldsymbol{S}^w}{\partial y}\right) \right] \delta\bar{\boldsymbol{u}} \tag{4.15}$$

$$\delta^2\gamma_{xy} = \delta\bar{\boldsymbol{u}}^\top \left[\left(\frac{\partial \boldsymbol{S}^u}{\partial x}\right)^\top \left(\frac{\partial \boldsymbol{S}^u}{\partial y}\right) + \left(\frac{\partial \boldsymbol{S}^u}{\partial y}\right)^\top \left(\frac{\partial \boldsymbol{S}^u}{\partial x}\right) \right. \tag{4.16}$$

$$+ \left(\frac{\partial \boldsymbol{S}^v}{\partial x}\right)^\top \left(\frac{\partial \boldsymbol{S}^v}{\partial y}\right) + \left(\frac{\partial \boldsymbol{S}^v}{\partial y}\right)^\top \left(\frac{\partial \boldsymbol{S}^v}{\partial x}\right) \tag{4.17}$$

$$\left. + \left(\frac{\partial \boldsymbol{S}^w}{\partial x}\right)^\top \left(\frac{\partial \boldsymbol{S}^w}{\partial y}\right) + \left(\frac{\partial \boldsymbol{S}^w}{\partial y}\right)^\top \left(\frac{\partial \boldsymbol{S}^w}{\partial x}\right) \right] \delta\bar{\boldsymbol{u}} \tag{4.18}$$

Then:

$$\delta\bar{\boldsymbol{u}}^\top \boldsymbol{K}_G \delta\bar{\boldsymbol{u}} = \delta\bar{\boldsymbol{u}}^\top \int_\Omega \hat{\sigma}_{xx} \left(\frac{\partial \boldsymbol{S}^u}{\partial x}\right)^\top \left(\frac{\partial \boldsymbol{S}^u}{\partial x}\right) + \hat{\sigma}_{xx} \left(\frac{\partial \boldsymbol{S}^v}{\partial x}\right)^\top \left(\frac{\partial \boldsymbol{S}^v}{\partial x}\right) + \hat{\sigma}_{xx} \left(\frac{\partial \boldsymbol{S}^w}{\partial x}\right)^\top \left(\frac{\partial \boldsymbol{S}^w}{\partial x}\right)$$

$$+\hat{\sigma}_{yy} \left(\frac{\partial \boldsymbol{S}^u}{\partial y}\right)^\top \left(\frac{\partial \boldsymbol{S}^u}{\partial y}\right) + \hat{\sigma}_{yy} \left(\frac{\partial \boldsymbol{S}^v}{\partial y}\right)^\top \left(\frac{\partial \boldsymbol{S}^v}{\partial y}\right) + \hat{\sigma}_{yy} \left(\frac{\partial \boldsymbol{S}^w}{\partial y}\right)^\top \left(\frac{\partial \boldsymbol{S}^w}{\partial y}\right)$$

$$+\hat{\tau}_{xy} \left(\frac{\partial \boldsymbol{S}^u}{\partial x}\right)^\top \left(\frac{\partial \boldsymbol{S}^u}{\partial y}\right) + \hat{\tau}_{xy} \left(\frac{\partial \boldsymbol{S}^u}{\partial y}\right)^\top \left(\frac{\partial \boldsymbol{S}^u}{\partial x}\right)$$

$$+\hat{\tau}_{xy} \left(\frac{\partial \boldsymbol{S}^v}{\partial x}\right)^\top \left(\frac{\partial \boldsymbol{S}^v}{\partial y}\right) + \hat{\tau}_{xy} \left(\frac{\partial \boldsymbol{S}^v}{\partial y}\right)^\top \left(\frac{\partial \boldsymbol{S}^v}{\partial x}\right)$$

$$+\hat{\tau}_{xy} \left(\frac{\partial \boldsymbol{S}^w}{\partial x}\right)^\top \left(\frac{\partial \boldsymbol{S}^w}{\partial y}\right) + \hat{\tau}_{xy} \left(\frac{\partial \boldsymbol{S}^w}{\partial y}\right)^\top \left(\frac{\partial \boldsymbol{S}^w}{\partial x}\right) d\Omega\, \delta\bar{\boldsymbol{u}}$$

$\hat{\sigma}_{xx}, \hat{\sigma}_{yy}, \hat{\tau}_{xy}$ can be calculated for plate elements from an initial nodal displacement state $\hat{\boldsymbol{u}}$ (fundamental or pre-buckling state) as:

$$\begin{Bmatrix} \hat{\sigma}_{xx} \\ \hat{\sigma}_{yy} \\ \hat{\tau}_{xy} \end{Bmatrix} = \frac{1}{h} \begin{bmatrix} \boldsymbol{A} & \boldsymbol{B} \\ \boldsymbol{B} & \boldsymbol{D} \end{bmatrix} \left(\boldsymbol{B}_L + \frac{1}{2}\boldsymbol{B}_{NL} \right) \hat{\boldsymbol{u}}$$

applying the van K'arm'an simplifications, $\delta^2\boldsymbol{\varepsilon}$ is defined as:

$$\delta^2\varepsilon_{xx} = \delta w_{,x}\delta w_{,x}\delta^2\varepsilon_{yy} \quad = \delta w_{,y}\delta w_{,y}\delta^2\gamma_{xy} = 2\delta w_{,x}\delta w_{,y}$$

using finite element or Ritz shape functions:

$$\delta^2\varepsilon_{xx} = \delta\bar{\boldsymbol{u}}^\top \left[\left(\frac{\partial \boldsymbol{S}^w}{\partial x}\right)^\top \left(\frac{\partial \boldsymbol{S}^w}{\partial x}\right) \right] \delta\bar{\boldsymbol{u}} \tag{4.19}$$

$$\delta^2\varepsilon_{yy} = \delta\bar{\boldsymbol{u}}^\top \left[\left(\frac{\partial \boldsymbol{S}^w}{\partial y}\right)^\top \left(\frac{\partial \boldsymbol{S}^w}{\partial y}\right) \right] \delta\bar{\boldsymbol{u}} \tag{4.20}$$

$$\delta^2\gamma_{xy} = \delta\bar{\boldsymbol{u}}^\top \left[\left(\frac{\partial \boldsymbol{S}^w}{\partial x}\right)^\top \left(\frac{\partial \boldsymbol{S}^w}{\partial y}\right) + \left(\frac{\partial \boldsymbol{S}^w}{\partial y}\right)^\top \left(\frac{\partial \boldsymbol{S}^w}{\partial x}\right) \right] \delta\bar{\boldsymbol{u}} \tag{4.21}$$

Then:

$$\delta\bar{\boldsymbol{u}}^\top \boldsymbol{K}_G \delta\bar{\boldsymbol{u}} = \delta\bar{\boldsymbol{u}}^\top \int_\Omega \hat{\sigma}_{xx} \left(\frac{\partial \boldsymbol{S}^w}{\partial x}\right)^\top \left(\frac{\partial \boldsymbol{S}^w}{\partial x}\right)$$

$$+\hat{\sigma}_{yy} \left(\frac{\partial \boldsymbol{S}^w}{\partial y}\right)^\top \left(\frac{\partial \boldsymbol{S}^w}{\partial y}\right)$$

$$+\hat{\tau}_{xy} \left(\frac{\partial \boldsymbol{S}^w}{\partial x}\right)^\top \left(\frac{\partial \boldsymbol{S}^w}{\partial y}\right) + \hat{\tau}_{xy} \left(\frac{\partial \boldsymbol{S}^w}{\partial y}\right)^\top \left(\frac{\partial \boldsymbol{S}^w}{\partial x}\right) d\Omega\, \delta\bar{\boldsymbol{u}}$$

$\hat{\sigma}_{xx}, \hat{\sigma}_{yy}, \hat{\tau}_{xy}$ can be calculated for plate elements from an initial nodal displacement state $\hat{\boldsymbol{u}}$ (fundamental or pre-buckling state) as:

$$\begin{Bmatrix} \hat{\sigma}_{xx} \\ \hat{\sigma}_{yy} \\ \hat{\tau}_{xy} \end{Bmatrix} = \frac{1}{h} \begin{bmatrix} \boldsymbol{A} & \boldsymbol{B} \\ \boldsymbol{B} & \boldsymbol{D} \end{bmatrix} \left(\boldsymbol{B}_L + \frac{1}{2}\boldsymbol{B}_{NL}\right) \hat{\boldsymbol{u}}$$

4.2 Buckling of a plate using full 3D elasticity

For the 3D elasticity case, the following expression can be used to calculate the geometric stiffness matrix for plates, using van Kármán kinematics:

$$\begin{aligned} \mathbf{K}_G = \iiint_{x,y,z} \Bigg[& \hat{\sigma}_{xx} \left(\frac{\partial \boldsymbol{S}^w}{\partial x}\right)^\top \left(\frac{\partial \boldsymbol{S}^w}{\partial x}\right) \\ & +\hat{\sigma}_{yy} \left(\frac{\partial \boldsymbol{S}^w}{\partial y}\right)^\top \left(\frac{\partial \boldsymbol{S}^w}{\partial y}\right) \\ & +\hat{\sigma}_{xy} \left(\frac{\partial \boldsymbol{S}^w}{\partial x}\right)^\top \left(\frac{\partial \boldsymbol{S}^w}{\partial y}\right) \\ & +\hat{\sigma}_{xy} \left(\frac{\partial \boldsymbol{S}^w}{\partial y}\right)^\top \left(\frac{\partial \boldsymbol{S}^w}{\partial x}\right) \Bigg] dxdydz \end{aligned}$$

An example on how to implement buckling of aplate using full 3D elasticity and the Ritz Method can be found in this notebook.

4.3 Buckling of a plate using the CLPT, FSDT or TSDT

For all 3 equivalent single-layer (ESL) theories previously discussed, the following expression can be used to calculate the geometric stiffness matrix for plates, using van Kármán kinematics:

$$\begin{aligned}\boldsymbol{K}_G = \iint_{x,y}^{\square} \widehat{N}_{xx} \left(\frac{\partial \boldsymbol{S}^w}{\partial x}\right)^{\mathsf{T}} \left(\frac{\partial \boldsymbol{S}^w}{\partial x}\right) \\ + \widehat{N}_{yy} \left(\frac{\partial \boldsymbol{S}^w}{\partial y}\right)^{\mathsf{T}} \left(\frac{\partial \boldsymbol{S}^w}{\partial y}\right) \\ + \widehat{N}_{xy} \left(\frac{\partial \boldsymbol{S}^w}{\partial x}\right)^{\mathsf{T}} \left(\frac{\partial \boldsymbol{S}^w}{\partial y}\right) \\ + \widehat{N}_{xy} \left(\frac{\partial \boldsymbol{S}^w}{\partial y}\right)^{\mathsf{T}} \left(\frac{\partial \boldsymbol{S}^w}{\partial x}\right) dxdy\end{aligned}$$

An example on how to implement buckling of aplate using the FSDT and the Ritz Method can be found in this notebook.

This page is intentionally left blank.

Table 1: Post-Buckling Characteristics for Various Loading Conditions

Loading Type	Post-Buckling Pattern	Stability/Behavior
Pure Compression	Diamond-shaped	Highly unstable; snapping occurs with decreasing N.
Pure Torsion	Diagonal-shaped	Smooth path; load carrying capacity usually decreases.
Torsion + Pre-tension	Diagonal-shaped	Pre-tension increases the critical load and stabilizes the path.
Torsion + Pre-compression	Twisted Diamond	Large pre-compression triggers snapping and complex pattern transitions.

5 Linear buckling of shells with general boundary conditions

5.1 Linear buckling of cylindrical shells under compression and torsion

Under pure compression, the shell buckles into an axisymmetric or diamond-shaped pattern (Yoshimura pattern), whereas under pure torsion, the shell deforms into a diagonal-shaped pattern with spiral wrinkles. Castro et al. (Castro et al., 2014) and Lu et al. (Lu et al., 2025) explores how these modes interact under combined loads, such as compression with pre-torsion or torsion with pre-compression. The interaction of axial and torsional loads creates a rich variety of behaviors:

The next sections will discuss different implementations of this shell buckling problem.

This page is intentionally left blank.

6 Post-buckling of plates

While historically buckling was seen as failure, modern engineering recognizes the postbuckling reserve of stiffened panels. These panels can withstand loads significantly exceeding their initial buckling threshold by allowing local buckling of the skin while stiffeners maintain global integrity.

6.1 Differential quadrature

Methodological Comparison: DQM, iDQM, and MiDQM

When solving high-order boundary value problems such as the coupled Föppl--von Kármán (FvK) equations, the choice of spatial discretization dictates the numerical stability of the solver. We can categorize the Differential Quadrature (DQ) family into three distinct approaches.

6.1.1 Pure direct Differential Quadrature Method (DQM)

TODO highlight the strong form

Pure DQM directly approximates the derivatives of a function at a set of grid points using a weighted linear sum of the function values at all other points. Higher-order derivative matrices are computed by simple matrix multiplication of the first-order weighting matrix ($D^{(m)} = D^{(1)} \dots D^{(1)}$).

Characteristics: Extremely simple to implement.

Drawback: As noted by Raju et al. (2013) (Raju et al., 2013), Pure DQM is notorious for numerical instability in highly nonlinear post-buckling problems. The condition number of $D^{(m)}$ scales exponentially with m and the number of grid points N.

6.1.2 Pure inverse Differential Quadrature Method (iDQM)

Proposed by Ojo et al. (2021) (Ojo et al., 2021), the Pure iDQM inverts the mathematical logic of DQM. Instead of approximating the function and differentiating, it directly approximates the highest-order derivative (e.g., $W_{,xxxx}$) using standard DQ. The lower-order derivatives and the function itself are recovered via integration weighting matrices ($H^{(m)}$), utilizing boundary conditions as constants of integration.

Characteristics: Requires the formulation of inverse boundary value problems to define the integration constants analytically.

Advantage: Integration is inherently a smoothing operation, meaning the condition number of the resulting algebraic system is significantly reduced.

Let's critically evaluate the motivation of Ojo et al. (2021) (Ojo et al., 2021). Ojo et al. proposed the iDQM fundamentally to bypass the extreme ill-conditioning and round-off error amplification caused by high-order differentiation matrices ($D^{(4)}$) in Pure DQM. When the condition number hits $\mathcal{O}(10^8)$, standard numerical solvers fail to converge. While Ojo's mathematical diagnosis of the matrix condition number is correct, their conclusion that one must switch to integral matrices to achieve stability in high-order PDEs is a misdiagnosis of where the failure actually occurs in nonlinear structural solvers.

Take an analytical Airy stress-based DQM, such as the one implemented in this practice, where Ojo's motivation is fundamentally bypassed. The instability in standard Pure DQM for FvK equations is rarely caused by a static matrix-vector multiplication $D^{(4)}W$. The failure actually occurs inside the Newton-Raphson solver during the finite-difference approximation of the Jacobian.

When a standard optimizer perturbs the state vector by $\epsilon = 10^{-7}$, the $\mathcal{O}(10^8)$ condition number of $D^{(4)}$ amplifies this perturbation into massive $\mathcal{O}(0.1)$ numeric noise, destroying the descent direction. By deriving the exact analytical Jacobian using Kronecker tensor products, rhe finite-difference noise is entirely eliminated. Consequently, the Pure DQM achieves machine-precision convergence instantly, rendering the heavy machinery of integral H-matrices (iDQM) unnecessary.

When using the Ritz-DQM, Ojo's motivation also becomes invalid. Ojo's premise relies on the instability of 4^{th}-order derivatives in the strong form. The Ritz method, however, operates on the Total Potential Energy (Π), which is the weak form. Furthermore, a lower derivative order is achieved with integration by parts when compared to the strong from, reducing the highest spatial derivative to $m = 2$ (the bending curvatures $\kappa_{x,y}$), fundamentally reducing the numerical instability. Finally, the Ritz-DQM does not use dense, global differentiation matrices $D^{(m)}$. Instead, in the practice herein proposed, an analytical, hierarchical Legendre basis functions are proposed, which allow exact analytical derivatives to be calculated at Gauss-Legendre integration points. Because Ritz-DQM relies on exact polynomial derivatives and exact numerical quadrature, it entirely circumvents the round-off amplification issues that Ojo et al. aimed to solve with the inverse quadrature method.

6.1.3 Mixed iDQM (MiDQM)

TODO find more about this

MiDQM is a hybrid approach discussed in contemporary literature (including extensions of Ojo et al.). It uses direct differentiation matrices ($D^{(m)}$) for lower-order derivative terms and integration matrices ($H^{(m)}$) for the highest-order terms.

Characteristics: Balances the smoothing benefits of integral operators with the straightforward boundary condition enforcement of standard differentiation.

6.2 Differential quadrature (OLD)

The Differential Quadrature Method (DQM) is a global numerical technique used to solve partial differential equations (PDEs). Unlike the Finite Element Method (FEM) which relies on localized piecewise interpolation, DQM approximates the derivative of a function at a specific grid point as a weighted linear sum of the function values at all discrete points in the domain.

For a 1D function $f(x)$ discretized over N points, the n-th order derivative at point x_i is given by:

$$\left.\frac{d^n f}{dx^n}\right|_{x=x_i} = \sum_{j=1}^{N} W_{ij}^{(n)} f(x_j) \quad \text{for } i = 1, 2, \ldots, N$$

where $W_{ij}^{(n)}$ are the weighting coefficients. To suppress Runge's phenomenon at higher polynomial orders, the grid points are not distributed uniformly, but rather follow the roots of orthogonal polynomials, such as Chebyshev-Gauss-Lobatto or Gauss-Legendre grids. While traditional DQM solves the strong form of the governing PDEs directly at the collocation points, this approach is mathematically brittle for 2D plate boundaries (specifically corners) due to linearly dependent constraints.

6.2.1 The Ritz-DQ Method

To bypass corner singularities and maintain the exponential convergence of spectral methods, it's possible to transition to the **weak form** via the Ritz-DQ method, which hybridises the classical Ritz variational method with DQM's numerical integration rules. Instead of directly evaluating the PDEs, the Ritz-DQ method minimizes the Total Potential Energy (Π) of the system. The continuous displacement fields (u, v, w) are expanded using a spectral basis (Legendre polynomials).

The DQM machinery is then leveraged to evaluate the continuous energy integrals using exact Gauss-Legendre quadrature.

Approximation functions The transverse deflection $w(x, y)$ and in-plane displacements $u(x, y)$, $v(x, y)$ are approximated by expanding unknown Ritz coefficients $\mathbf{C}$ over 1D Legendre polynomials. To explicitly satisfy the simply supported (SSSS) kinematic boundary conditions ($w = 0$ at edges), the following modified Legendre basis can be constructued:

$$\phi_m(\xi) = P_{m+2}(\xi) - P_m(\xi)$$

Because standard Legendre polynomials $P_m(\pm 1) = (\pm 1)^m$, the difference exactly vanishes at the domain edges. The transverse field is thus:

$$w(\xi, \eta) = \sum_{i=0}^{N_c} \sum_{j=0}^{N_c} C_{ij}^w \phi_i(\xi) \phi_j(\eta)$$

Strain energy To capture post-buckling behavior, the strain-displacement relations must account for geometric nonlinearity. The von Karman mid-plane strains isolate the dominant transverse stiffening effects:

$$\begin{aligned} \varepsilon_{xx} &= u_{,x} + \frac{1}{2} w_{,x}^2 \\ \varepsilon_{yy} &= v_{,y} + \frac{1}{2} w_{,y}^2 \\ \gamma_{xy} &= u_{,y} + v_{,x} + w_{,x} w_{,y} \end{aligned}$$

The Total Potential Energy (Π) is the sum of the membrane (U_m) and bending (U_b) strain energies. Defining extensional stiffness $C_{ext} = \frac{Eh}{1-\nu^2}$ and bending stiffness $D = \frac{Eh^3}{12(1-\nu^2)}$:

$$U_m = \frac{C_{ext}}{2} \int_A \left(\varepsilon_{xx}^2 + \varepsilon_{yy}^2 + 2\nu \varepsilon_{xx} \varepsilon_{yy} + \frac{1-\nu}{2} \gamma_{xy}^2 \right) dA$$

$$U_b = \frac{D}{2} \int_A \left(w_{,xx}^2 + w_{,yy}^2 + 2\nu w_{,xx} w_{,yy} + 2(1-\nu) w_{,xy}^2 \right) dA$$

In the Ritz-DQM, the continuous integral $\int_A (\dots) dA$ is replaced by the 2D Gauss-Legendre quadrature summation $\sum\sum (\dots) W_{ij}$.

An example of the Ritz-DQ method can be seen in this notebook.

6.3 Effective width

The postbuckling behavior and stress/strain distribution of stiffened panels is complex and non-linear. Complicated non-linear numerical calculation methods that employ sig- nificant computational resources are laborious and are required to confidently predict the panels ultimate load capacity (Pevzner et al., 2008). To alleviate the calculations, a relatively simplified model, the so called ``effective width'' approach, has been proposed by von K'arman et al. (von Kármán et al., 1932) and subsequently modified by Cox (Cox, 1933) and Sechler (Sechler, 1937). This approach has provided a good average approximation for calculation of the effective width, w_e, i.e. the portion of the between adjacent stringers buckled skin, that together with the stringer constitute the integral skin-stringer combi- nation that participates in load carrying in postbuckling. The method works adequately for the case of uniaxial compression, and it is not recommended when there is biaxial loading or compression combined with shear (Kassapoglou, 2013). Based on the average stress

s_{st} experienced by the stringers and the first critical skin stress, s_{cr} between adjacent stringers of spacing b, the following relation has been pro- posed by Marguerre for determination of w_e:

$$\frac{w_e}{b} = \frac{1}{2}\sqrt[3]{\frac{s_{cr}}{s_{st}}} \tag{6.1}$$

The above effective width concept is widely and effectively applied as an adequate reliable tool for prediction of ultimate loads of metal flat stiffened panels. When appropriately modified and adapted it might lend itself as an appropriate approach for determination of ultimate load capacities of axially compressed laminated composite stringer-stiffened curved panels as well (Pevzner et al., 2008).

The effective width method simplifies the complex and non-uniform stress distribution in a buckled panel, replacing it with an equivalent and uniform stress acting over a reduced ``effective width'' of the skin adjacent to the stiffeners.

6.3.1 Effective width for metallic structures

6.3.2 Effective width for composite plates

An example on how the effective width changes with the loading fraction and material properties can be seen in this notebook. An illustration on how the internal load changes over the skin width can be found in this other notebook

6.3.3 Effective width for composite shells

The Technion Effective Width (TEW) method (Pevzner et al., 2008) is an engineering approximation for analyzing the postbuckling behavior of curved, laminated composite structures. The TEW method extends the effective width concept to curved, anisotropic, laminated composite panels by reformulating an equivalent column model to account for the unique bending, torsional, and coupled instability modes of composite structures.

The TEW analysis process is summarized as follows:

1. **First Buckling Calculation**: Determining the initial local buckling of the skin between stringers using semi-empirical or approximate analytical solutions.
2. **Iterative Convergence of Effective Width**: Once the load exceeds the initial buckling load, an iterative algorithm calculates the effective width of the skin contributing to the load-carrying capacity. This process continues until the stress redistribution between the buckled skin and the stiffener reaches equilibrium.
3. **Global Stability Analysis**: Evaluating the global column stability based on the flexural, torsional, and warping rigidities of the equivalent skin-stringer cross-section to determine the ultimate collapse load.

An example of the TEW method is presented in this notebook.

The TEW paper reveals that the predictive fidelity of the TEW method is closely linked to the panel's stiffness.

Configuration & Geometry	P_buckling (kN) (Experiment)	P_collapse (kN) (Experiment)	P_collapse (kN) (F.E. Method)	P_collapse (kN) (Proposed TEW Method)
Case I: 5 T-type, 20 mm web	137.3, 147.2, 158.5	208.7, 222.7, 224.8	204.0	240.5
Case II: 5 T-type, 15 mm web	133.4, 110.9, 123.6	158.9, 153.3, 147.2	135.0	127.4
Case III: 6 T-type, 20 mm web	224.2, 237.3, 234.5	274.7, 264.9, 274.7	290.0	281.7
Case IV: 5 J-form thin stringers	83.4, 70.6	230.5, 226.1	215.0	202.6
Case V: 4 J-form thick stringers	59.8, 90.8	289.8, 293.0	330.0	354.9

- **Heavily Stiffened Panels (Cases I, V)**: The TEW method tends to overpredict the collapse load. This is likely because the model does not capture localized failure modes like skin-stiffener debonding that can occur before global buckling.
- **Lightly Stiffened Panels (Cases II, IV)**: The TEW method tends to conservatively underpredict the collapse load. The small margin between initial skin buckling and global collapse in these flexible structures may lead the algorithm to predict failure prematurely.
- **Asymmetric Stiffeners (Cases IV, V)**: The use of J-form stringers introduces coupled bending-torsion modes, which significantly complicates the buckling behavior and increases sensitivity to manufacturing imperfections.

This page is intentionally left blank.

7 Post-buckling of perfect shells

For shells, the coupling between the normal deflection and membrane strains create more intricate kinematic relations and require that at least two field variables are solved simultaneously. In cylindrical shells it is possible to resolve the buckling or geometrically non-linear displacement by using only the hoop and normal displacements, which are coupled in the hoop strain term. Another approach consists of the hybrid Airy' stress-based formulation in which the normal displacement and the Airy stress function are approximated. From the Airy stress function the membrane stresses can be readily derived, and thus the total potential of the system can be constructed and solved.

7.1 Galerkin method using Airy's stress function

The method herein presented is based on the recent work of Lu et al. (Lu et al., 2025), developed for isotropic shells.

7.1.1 Core formulation

This part provides comprehensive theoretical overview of the buckling and post-buckling behavior of thin-walled cylindrical shells under single and combined loading conditions, based on the recent work of Lu et al. (Lu et al., 2025). The formulation follows the Donnell shell theory solved via the Galerkin method. The theoretical framework is established using Donnell shell theory, which is widely adopted for thin shells due to its practical accuracy and relative simplicity. It assumes that in-plane displacements are negligible compared to transverse displacements.

For a cylindrical shell of length L, radius R, and thickness h, the state is defined by the transverse displacement $w(x, y)$ and the Airy stress function $F(x, y)$. The balance of forces in the radial direction, considering geometric nonlinearities (von K'arm'an terms), is given by:

$$D\nabla^4 w - \frac{1}{R}\frac{\partial^2 F}{\partial x^2} = \frac{\partial^2 F}{\partial y^2}\frac{\partial^2 w}{\partial x^2} - 2\frac{\partial^2 F}{\partial x \partial y}\frac{\partial^2 w}{\partial x \partial y} + \frac{\partial^2 F}{\partial x^2}\frac{\partial^2 w}{\partial y^2}$$

where $D = \frac{Eh^3}{12(1-\nu^2)}$ is the flexural rigidity. To ensure a continuous displacement field, the stress function must satisfy:

$$\nabla^4 F + \frac{Eh}{R}\frac{\partial^2 w}{\partial x^2} = Eh\left[\left(\frac{\partial^2 w}{\partial x \partial y}\right)^2 - \frac{\partial^2 w}{\partial x^2}\frac{\partial^2 w}{\partial y^2}\right]$$

To solve these nonlinear partial differential equations (PDEs), Lu et al. transformed them into a system of algebraic equations using the Galerkin method. For clamped-clamped (C-C) boundary conditions, the dimensionless transverse displacement $\bar{w}$ is assumed as a double Fourier series:

$$\bar{w}(\bar{x}, \bar{y}) = \sum_{m=1}^{\infty}\sum_{n=0}^{\infty} a_{m,n}(\psi_{m-1,n} + \psi_{m+1,n})$$

where ψ_{mn} are basis functions that inherently satisfy the boundary conditions:

$$\psi_{mn} = \cos(m\bar{x} + n\bar{y}) + (-1)^m \cos(m\bar{x} - n\bar{y})$$

To derive the stress function, the $\bar{w}$ approximation is inserted into the compatibility equation, allowing the analytical determination of the stress function F in terms of the unknown modal

amplitudes $a_{m,n}$. Applying the Galerkin procedure to the equilibrium equation yields a coupled system of cubic algebraic equations:

$$\int_0^{2\pi} \int_{-\pi/2}^{\pi/2} \mathcal{J}(\bar{w}, f)(\psi_{r-1,s} + \psi_{r+1,s}) d\bar{x} d\bar{y} = 0$$

7.1.2 Stability and non-linear path tracking

Tracking the post-buckling equilibrium path requires advanced numerical strategies to handle instabilities and multi-valued solutions. Standard load-controlled solvers fail at limit points where the shell ``snaps'' to a new state. The arc-length method (Riks method) parameterizes the path by a distance $s$ along the curve, treating the load parameter ($\Sigma$ or $k_s$) as an additional unknown. This allows the solver to trace unstable ``snap-back'' branches where both load and displacement decrease simultaneously. The stability of a branch is determined by the Jacobian matrix ($\mathbf{J}$) of the residual system, and can be classified within the following criteria:

- Stability criterion: A branch is stable if all eigenvalues of $\mathbf{J}$ have positive real parts.
- Bifurcation/Limit Points: These occur when the minimum real eigenvalue crosses zero ($\lambda_{min} \approx 0$).
- Mode Jumping: Physically, the shell snaps to a lower energy state, often characterized by a decrease in the circumferential wavenumber N.

7.1.3 Non-dimensionalisation scheme

To generalize the computational model across varying geometries, Lu et al. (Lu et al., 2025) proposed a normalisation of the PDEs. The physical domain is mapped into a dimensionless space using the circumferential wavenumber N.

Spatial coordinates and field variables:

- Axial Coordinate: $\bar{x} = \frac{\pi x}{L}$
- Circumferential Coordinate: $\bar{y} = \frac{Ny}{R}$
- Transverse Displacement: $\bar{w} = \frac{w}{h}$
- Airy's Stress Function: $f = \frac{F}{Eh^3}$

The shell's properties are condensed into dimensionless constants:

- Normalized flexural rigidity constant based on Poisson's ratio ν: $c = \frac{1}{12(1-\nu^2)}$
- Geometric scaling factor dependent on the length-to-radius and radius-to-thickness ratios: $\alpha = \frac{L^2}{\pi^2 Rh}$
- Dimensionless parameter associated with the circumferential wavenumber N: $\beta = \frac{NL}{\pi R}$

The external loads and global deformations are scaled to trace the equilibrium paths:

- Dimensionless Axial Force: $k_x = \frac{PL^2}{2\pi^3 ERh^3}$
- Dimensionless Torque: $k_s = \frac{TL^2}{2\pi^3 R^2 D}$
- Dimensionless End Shortening: $\bar{\delta} = \frac{R\Delta}{Lh}$

- Dimensionless Twisting Angle: $\bar{\varphi} = \frac{R^2\varphi}{Lh}$

In force-control scenarios, the compressive force P is frequently normalized against the classical critical buckling load P_{cr0} for simply supported shells, denoted as $\Sigma = P/P_{cr0}$. This relates to the core parameter via $P/P_{cr0} = \sqrt{3(1-\nu^2)}\frac{k_x}{\alpha}$.

7.2 Practice, Galerkin method using Airy's stress function

This notebook.

This page is intentionally left blank.

8 Post-buckling of shells with imperfections

For shells with imperfections ... TODO

8.1 TODO link to Zenodo imperfection database

Appendices

A Shear Correction Factors

When the FSDT is used, constant transverse shear strains γ_{yz} and γ_{xz} are assumed, as detailed in Section 2.6.6, creating an inconsistent transverse shear energy in the system, and therefore requiring a so called and widely used shear correction factor (SCF). The wide application comes from FSDT-based plate elements being the most popular in commercial finite element software.

This page is intentionally left blank.

References

N. Bardell. Free vibration analysis of a flat plate using the hierarchical finite element method. *Journal of Sound and Vibration*, 151(2):263--289, 12 1991. ISSN 0022-460X. doi:10.1016/0022-460x(91)90855-e. URL http://dx.doi.org/10.1016/0022-460X(91)90855-E.

N. Bardell, J. Dunsdon, and R. Langley. Free and forced vibration analysis of thin, laminated, cylindrically curved panels. *Composite Structures*, 38(1--4):453--462, 5 1997a. ISSN 0263-8223. doi:10.1016/s0263-8223(97)00080-9. URL http://dx.doi.org/10.1016/S0263-8223(97)00080-9.

N. Bardell, J. Dunsdon, and R. Langley. On the free vibration of completely free, open, cylindrically curved, isotropic shell panels. *Journal of Sound and Vibration*, 207(5):647--669, 11 1997b. ISSN 0022-460X. doi:10.1006/jsvi.1997.1115. URL http://dx.doi.org/10.1006/jsvi.1997.1115.

S. G. Castro and M. V. Donadon. Assembly of semi-analytical models to address linear buckling and vibration of stiffened composite panels with debonding defect. *Composite Structures*, 160: 232--247, 1 2017. ISSN 0263-8223. doi:10.1016/j.compstruct.2016.10.026. URL http://dx.doi.org/10.1016/j.compstruct.2016.10.026.

S. G. Castro, C. Mittelstedt, F. A. Monteiro, M. A. Arbelo, G. Ziegmann, and R. Degenhardt. Linear buckling predictions of unstiffened laminated composite cylinders and cones under various loading and boundary conditions using semi-analytical models. *Composite Structures*, 118: 303--315, 12 2014. ISSN 0263-8223. doi:10.1016/j.compstruct.2014.07.037. URL http://dx.doi.org/10.1016/j.compstruct.2014.07.037.

S. G. Castro, C. Mittelstedt, F. A. Monteiro, M. A. Arbelo, R. Degenhardt, and G. Ziegmann. A semi-analytical approach for linear and non-linear analysis of unstiffened laminated composite cylinders and cones under axial, torsion and pressure loads. *Thin-Walled Structures*, 90:61--73, 5 2015a. ISSN 0263-8231. doi:10.1016/j.tws.2015.01.002. URL http://dx.doi.org/10.1016/j.tws.2015.01.002.

S. G. Castro, C. Mittelstedt, F. A. Monteiro, R. Degenhardt, and G. Ziegmann. Evaluation of non-linear buckling loads of geometrically imperfect composite cylinders and cones with the Ritz method. *Composite Structures*, 122:284--299, 4 2015b. ISSN 0263-8223. doi:10.1016/j.compstruct.2014.11.050. URL http://dx.doi.org/10.1016/j.compstruct.2014.11.050.

S. G. P. Castro. Semi-analytical tools for the analysis of laminated composite cylindrical and conical imperfect shells under various loading and boundary conditinos, 2015.

S. G. P. Castro. Stability of Structures: Kinematics, Equivalent Single-Layer Theories, and Energy-based Semi-Analytical Methods, 2025.

H. L. Cox. The Buckling of Thin Plates in Compression. Reports and Memoranda 1554, Aeronautical Research Committee, London, 1933.

Z. De-Chao. *Development of Hierarchal Finite Element Methods at BIAA*, pages 159--164. Springer Japan, 1986. ISBN 9784431680420. doi:10.1007/978-4-431-68042-0_17. URL http://dx.doi.org/10.1007/978-4-431-68042-0_17.

C. Kassapoglou. *Design and Analysis of Composite Structures: With Applications to Aerospace Structures*. Wiley, 5 2013. ISBN 9781118536933. doi:10.1002/9781118536933. URL http://dx.doi.org/10.1002/9781118536933.

L. Lu, S. Leanza, Y. Liu, and R. R. Zhao. Buckling and post-buckling of cylindrical shells under combined torsional and axial loads. *European Journal of Mechanics - A/Solids*, 112:105653, 7 2025. ISSN 0997-7538. doi:10.1016/j.euromechsol.2025.105653. URL http://dx.doi.org/10.1016/j.euromechsol.2025.105653.

S. O. Ojo, L. C. Trinh, H. M. Khalid, and P. M. Weaver. Inverse differential quadrature method: mathematical formulation and error analysis. *Proceedings of the Royal Society A: Mathematical, Physical and Engineering Sciences*, 477(2248), 4 2021. ISSN 1471-2946. doi:10.1098/rspa.2020.0815. URL http://dx.doi.org/10.1098/rspa.2020.0815.

A. Peano. Hierarchies of conforming finite elements for plane elasticity and plate bending. *Computers & Mathematics with Applications*, 2(3--4):211--224, 1976. ISSN 0898-1221. doi:10.1016/0898-1221(76)90014-6. URL http://dx.doi.org/10.1016/0898-1221(76)90014-6.

P. Pevzner, H. Abramovich, and T. Weller. Calculation of the collapse load of an axially compressed laminated composite stringer-stiffened curved panel--An engineering approach. *Composite Structures*, 83(4):341--353, 6 2008. ISSN 0263-8223. doi:10.1016/j.compstruct.2007.05.001. URL http://dx.doi.org/10.1016/j.compstruct.2007.05.001.

G. Raju, Z. Wu, and P. M. Weaver. Postbuckling analysis of variable angle tow plates using differential quadrature method. *Composite Structures*, 106:74--84, 12 2013. ISSN 0263-8223. doi:10.1016/j.compstruct.2013.05.010. URL http://dx.doi.org/10.1016/j.compstruct.2013.05.010.

J. N. Reddy. *Mechanics of Laminated Composite Plates and Shells*. CRC Press, 11 2003. ISBN 9780429210693. doi:10.1201/b12409. URL http://dx.doi.org/10.1201/b12409.

E. E. Sechler. Stress Distribution in Stiffened Panels Under Compression. *Journal of the Aeronautical Sciences*, 4(8):320--323, 6 1937. ISSN 1936-9956. doi:10.2514/8.421. URL http://dx.doi.org/10.2514/8.421.

R. Vescovini, L. Dozio, M. D'Ottavio, and O. Polit. On the application of the Ritz method to free vibration and buckling analysis of highly anisotropic plates. *Composite Structures*, 192:460--474, 5 2018. ISSN 0263-8223. doi:10.1016/j.compstruct.2018.03.017. URL http://dx.doi.org/10.1016/j.compstruct.2018.03.017.

W. Voigt. *Lehrbuch der Kristallphysik (mit Ausschluss der Kristalloptik)*. Teubner, Leipzig, 1910.

T. von Kármán, E. E. Sechler, and L. H. Donnell. The Strength of Thin Plates in Compression. *Journal of Fluids Engineering*, 54(2):53--56, 1 1932. ISSN 0097-6822. doi:10.1115/1.4021738. URL http://dx.doi.org/10.1115/1.4021738.